Heat Transport by Topological Excitations

Pardeep Kumar Tanwar

Doctoral Dissertation

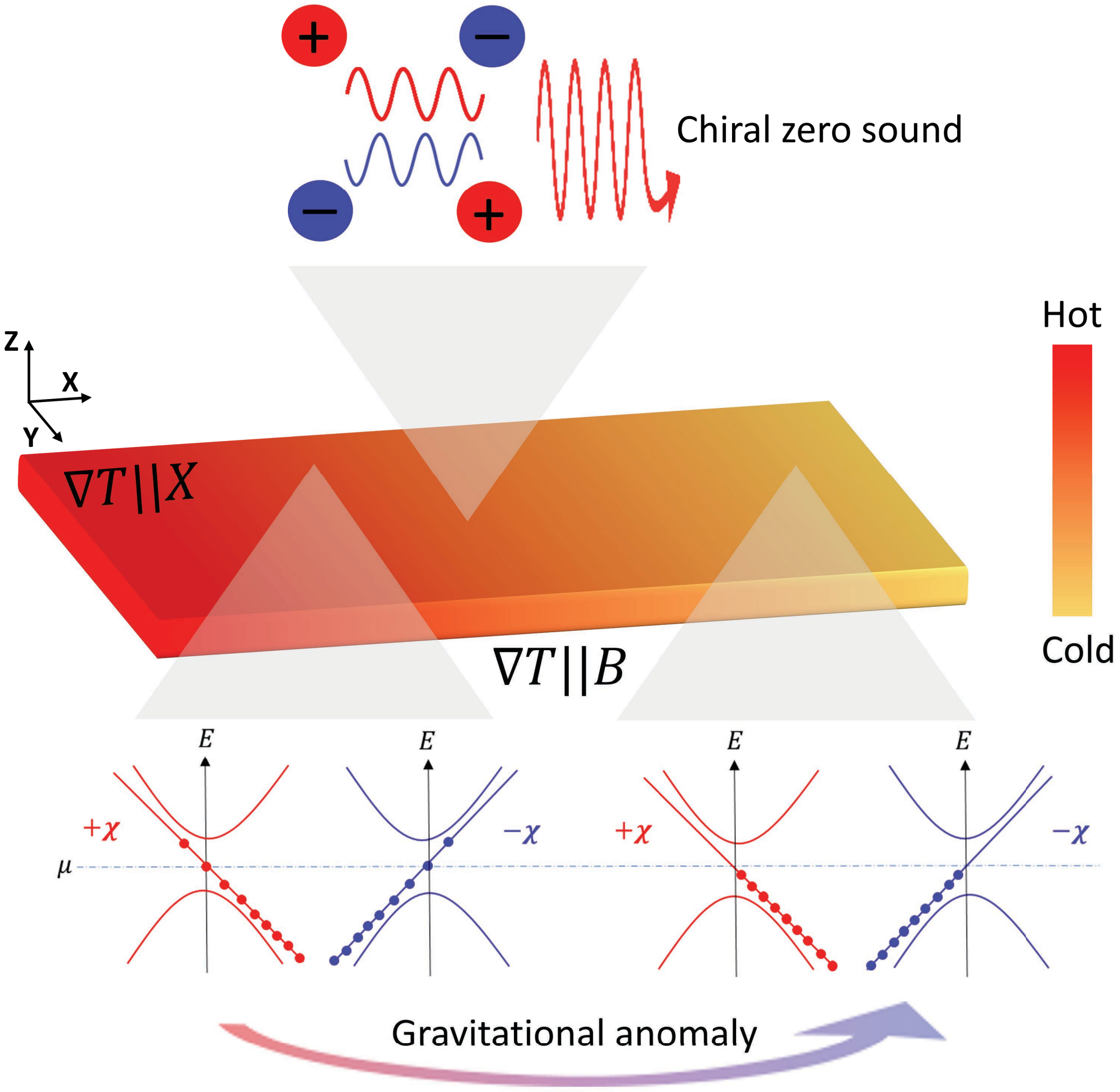

Heat Transport by Topological Excitations

Pardeep Kumar Tanwar

Doctoral Dissertation

April 2024

Cover photo: Schematic illustration of chiral zero sound and gravitational anomaly

Published by: International research centre MagTop
Institute of Physics Polish Academy of Sciences (IFPAN)
Aleja Lotników 32/46, 02-668
Warsaw, Poland
`www.ifpan.edu.pl`

Institute of Physics, Polish Academy of Sciences

DOCTORAL DISSERTATION

Heat Transport by Topological Excitations

Author

Pardeep Kumar Tanwar

Supervisor

Dr. hab. Marcin Matusiak

International Centre for Interfacing Magnetism and
Superconductivity with Topological Matter

April 2024

To my parents....

Preface

In the last two decades, the Weyl semimetal has been tremendously explored for searching the quantum effects such as chiral anomaly and anomalous Hall effect. However, the quantum effects remain largely uncharted through heat transport measurements. This PhD project, Heat Transport by Topological Excitations, aimed to probe the topological excitation through electrical and thermal conductivity measurements. The Ph.D. thesis was a joint project of Warsaw PhD School in Natural and BioMedical Sciences and International Research Centre MagTop, Institute of Physics, Polish Academy of Sciences (IFPAN), in partial fulfillment of the requirement to acquire a Doctor of Philosophy in physical sciences. The experimental work was carried out at MagTop, IFPAN, under the supervision of Dr. hab. Marcin Matusiak. The work presented in the thesis has been published in Physical Review B as letters and articles are attached, preceded by a brief summary.

Pardeep Kumar Tanwar

....

Signature

30 April 2024

....

Date

Reuse and Permissions License

In this thesis, I have attached my two first-author articles from Physical Review B (letter). I have obtained the necessary permissions from the journal (listed below).

- License Number: RNP/24/APR/078123
- License Number: RNP/24/APR/078124

Acknowledgements

I am filled with immense gratitude towards the individuals who have contributed to my journey toward obtaining my doctorate. Their support, guidance, and mentorship have significantly impacted my academic and personal growth. I want to extend my heartfelt appreciation to my supervisor, Dr. hab. Marcin Matusiak, for shaping my research direction with his insightful mentorship. I would like to express my sincere gratitude to Prof. Tomasz Dietl for the opportunity to be a part of his research group, the insightful discussion, and his timely guidance throughout the study. I would like to thank Prof. Tomasz Wojtowicz for becoming the acting supervisor in the absence of Dr. hab. Marcin Matusiak. I am thankful to Prof. Prof. Tomasz Story and Dr. hab. Krzysztof Dybko for allowing me to use their facilities. I would like to extend my sincere thanks to Prof. Dariusz Kaczorowski for the collaboration and fruitful discussions. I am also very grateful to Dr. Fazel Tafti and his lab members for their collaboration and insightful discussions. Additionally, I want to express my gratitude to Dr. Ekaterina Pomjakushina for accepting me as a visiting PhD student and for guidance during my stay at Paul Scherrer Institut PSI, Switzerland. Finally, I would like to give a special thanks to Dr. Dariusz Jakub Gawryluk for his support during my stay.

I would also like to thank my colleague Dr. Archana Mishra for numerous scientific and non-scientific thoughtful discussions. A special thanks to Dr. Ashutosh S. Wadge for the collaborative spirit and perceptive discussions that have enriched my research experience. The financial support from Warsaw PhD School in Natural and BioMedical Sciences, International Research Centre MagTop, Institute of Physics, Polish Academy of Sciences, and Erasmus+ has opened doors to critical opportunities, and I am truly grateful for their contribution. I am also thankful to my dear friends Sanjay Kapoor, Sarath Prem, and Dr. Sibananda Dash for their unwavering friendship that provided solace and joy amidst academic challenges. The efficient support of the administrative and technical staff of IFPAN has been invaluable.

I am incredibly blessed to have the love, support, and encouragement of my parents. Their unwavering dedication and effort are indescribable. They are always by my side, in every moment and everywhere. I am eternally grateful for everything they do. Without their support, I would not be able to pursue a career in science. My brother and sister always make every moment enjoyable. My niece and nephew are always curious about my work at distant places, and sometimes their questions are commendable. Last but not least, I owe a deep debt of gratitude to my partner, Dr. Neetu Lamba, for her unwavering love, understanding, and support throughout this journey. Her valuable insights and constructive feedback have helped me to present my work more effectively. Her company has been a constant source of inspiration and motivation for me, and I look forward to exploring more opportunities together.

Each of these individuals has left an indelible mark on my academic and personal development; I am genuinely grateful for that.

Achievements

List of publications

- **Tanwar, Pardeep Kumar**, M. S. Alam, M. Ahmad, D. Kaczorowski, and M. Matusiak, Severe violation of the Wiedemann-Franz law in quantum oscillations of NbP," Physical Review B (letter), vol. 106, no. 4, p. L041106, 2022.
- **Tanwar, Pardeep Kumar**, M. Ahmad, M. S. Alam, X. Yao, F. Tafti, and M. Matusiak, "Gravitational anomaly in the ferrimagnetic topological Weyl semimetal NdAlSi," Physical Review B (letter), vol. 108, no. 16, p. L161106, 2023.

List of presentations and external visit

- One month external research stay under Erasmus + program to grow single crystal Kitaev materials for heat transport, under the supervision of Dr. Ekaterina Pomjakushina, at Paul Scherrer Institute (PSI), Switzerland, 2023.
- "Thermal chiral (gravitational) anomaly in antiferromagnetic topological Weyl semimetal NdAlSi" at the American Physical Society (APS), March meeting, 2023, Las Vegas, USA (Contributed talk).
- "Thermal chiral anomaly in antiferromagnetic Weyl semimetal NdAlSi" at Northern Light Conference, 12-15 October 2022, Reykjavik, Iceland (poster).
- "Chiral zero sound: an additional heat channel in Weyl semimetal NbP." at Joint European Magnetic Symposia (JEMS), 24-29, July 2022, Warsaw, Poland (poster).
- "Severe violation of the Wiedemann-Franz law in quantum oscillations of NbP," Jaszowiec 2022, Poland (poster).

Other publications not included in the thesis

- **Tanwar, Pardeep Kumar**, A. S. Wadge, A. Balodhi, et al., "Additional heat channel topological magnon-polaron in Weyl semimetal NdAlSi," to be submitted, 2024.

- A. S. Wadge, K. Zberecki, B. J. Kowalski, D. Jastrzebski, **P. K. Tanwar**, et al., "Emergent impervious band crossing in the bulk in topological nodal line semimetal $ZrAs_2$," under review in Physical Review B.
- Alam, Md Shahin, Amar Fakhredine, Mujeeb Ahmad, **P. K. Tanwar**, Hung-Yu Yang, Fazel Tafti, Giuseppe Cuono, et al. "Sign change of anomalous Hall effect and anomalous Nernst effect in the Weyl semimetal CeAlSi." Physical Review B 107, no. 8 (2023): 085102.
- Alam, Md Shahin, **P. K. Tanwar**, Krzysztof Dybko, Ashutosh S. Wadge, Przemysaw Iwanowski, Andrzej Winiewski, and Marcin Matusiak. "Temperature-driven spin-zero effect in $TaAs_2$." Journal of Physics and Chemistry of Solids 170 (2022): 110939.

Abstract

Topological semimetals are materials with unique properties that hold great promise for use in high-speed electronics, next-generation spintronics, and quantum computing. Research to explore and understand the new quantum phenomena in these materials has recently become of considerable interest. The peculiar behavior of the semimetals is defined by their non-trivial linear band structure, where the relativistic nature of quasiparticles can be observed in low-energy excitations. The macroscopic consequences of the quantum phenomena are expected in charge and heat transport phenomena, such as the anomalous Hall effect and the chiral magnetic effect, which have been extensively studied. The latter effect is manifested as positive longitudinal magneto-electrical conductivity stemming from the chiral anomaly. However, the experimental study of this effect in electrical transport can be complicated by the occurrence of extrinsic effects such as the current jetting effect. On the other hand, the analogous form of chiral anomaly, the gravitational anomaly, is predicted to appear into heat transport, making its macroscopic consequences immune to such extrinsic effect as no external electric field is applied. Furthermore, thermal conductivity measurements are valuable in studying other topological excitations that are neither charge carriers nor phonons or magnons.

This dissertation presents the results of electrical and thermal transport studies of two Weyl semimetals, NbP and NdAlSi. In the former material, the results indicate the formation of a charge-neutral topological excitation called the chiral zero sound (CZS). Herein, huge quantum oscillations that appeared in thermal conductivity are ascribed as an additional heat channel due to CZS in the chiral limit. Consequently, these modes severely violate the Wiedemann-Franz (WF) law. In NdAlSi, a ferrimagnetic Weyl semimetal, the gravitational anomaly was the subject of study. This anomaly is postulated in quantum field theory describing the behavior of elementary particles and is

expected to be observable in Weyl semimetals. In our study, we observed an anomalous increase in magneto-electrical and -thermal conductivity in the semiclassical regime of NdAlSi. Remarkably, both anomalous changes in charge and thermal transport are related by the WF law.

This dissertation provides a better understanding of the topological properties and contributes to the search for a new type of non-trivial excitations in Weyl semimetals.

Streszczenie

Semimetale topologiczne są materiałami, których niezwykłe własności mogą być wykorzystane w szybkiej elektronice, spintronice nowej generacji i obliczeniach kwantowych. Badania mające na celu próbę zrozumienia nowego rodzaju zjawisk obserwowanych w tego typu związkach stały się ostatnio przedmiotem dużego zainteresowania. Okazuje się, że zachowanie semimetali topologicznych zdefiniowane jest przez ich nietrywialną liniową strukturę pasmową, gdzie w niskoenergetycznych wzbudzeniach można dojrzeć relatywistyczną naturę kwazicząstek. Jej makroskopowe przejawy można znaleźć w zjawiskach transportu ładunku i ciepła, wśród których anomalny efekt Halla i chiralny efekt magnetyczny były intensywnie badane. Drugi z efektów obserwowany jest jako dodatnie podłużne przewodnictwo magnetoelektryczne i związany jest z pojawianiem się anomalii chiralnej. Jej eksperymentalne badania mogą być jednak utrudnione ze względu na pojawianie się zjawisk, jak na przykład tzw. „current jetting effect", nie związanych z istotą fenomenu. Z drugiej strony istnieje możliwość obserwowania w transporcie ciepła grawitacyjnej anomalii kwantowej, której manifestacja powinna być odporna na tego typu zaburzenia. Wynika to z faktu, że eksperyment odbywa się bez przyłożenia zewnętrznego pola elektrycznego. Pomiary przewodności cieplnej okazują się także być nieocenione w badaniach innych wzbudzeń topologicznych nie będących ani nośnikami ładunku, ani fononami, czy też magnonami.

Niniejsza rozprawa opisuje badania transportu elektrycznego i cieplnego dwóch semimetali Weyla, a mianowicie NbP i NdAlSi. W pierwszym ze związków otrzymane wyniki wskazują na formowanie się neutralnego ładunkowo wzbudzenia topologicznego nazywanego chiralnym dźwiękiem zerowym (CSZ). Jego makroskopową manifestacją są obserwowane w przewodnictwie cieplnym bardzo duże oscylacje kwantowe. W tzw. limicie chiralnym CSZ stanowi dodatkowy kanał przepływu ciepła, przez co poważnie narusza prawo Wiedemanna-Franza. W drugim z materiałów, tj. ferrimagnetycznym semimetalu Weyla NdAlSi, przedmiotem badań było inne zjawisko kwantowe nazwane anomalią grawitacyjną. Pojawianie się tej anomalii postulowane jest w kwantowej teorii

pola opisującej zachowanie cząstek elementarnych i, co ciekawe, oczekuje się, że powinna ona być także obserwowalna np. w semimetalach Weyla. W naszych badaniach zauważyliśmy anomalny wzrost przewodnictwa magneto-elektrycznego i -termicznego w zakresie półklasycznym NdAlSi, przy czym zmiany transportu ładunkowego i cieplnego wydają się być związane prawem Wiedemanna-Franza.

Rozprawa przyczynia się do lepszego zrozumienia własności topologicznych i stanowi wkład w poszukiwanie nowego rodzaju nietrywialnych wzbudzeń.

Contents

List of Figures

Chapter 1

Introduction

This chapter briefly describes the role of topology in electronic band structures and introduces the Weyl semimetal phase. The intriguing transport characteristics of Weyl semimetal, such as negative magnetoresistance due to chiral anomaly, huge quantum oscillation in thermal conductivity caused by chiral zero sound modes, and positive magneto-thermal conductivity due to gravitational anomaly, are discussed. Additionally, electronic, lattice, and magnonic heat conduction mechanisms are covered.

1.1 Topology and electronic band structure

Topology is a mathematical concept that describes the characteristics of objects that remain preserved under continuous deformation, such as bending or twisting. For instance, a coffee mug can be transformed into a donut while keeping the same number of holes, which is a topological invariant. Here, coffee cups and donuts are considered topologically identical. However, these objects are topologically different from a pretzel (as it has three holes).

The study of topology in electronic band structures is an intriguing field for discovering new quantum phases of matter, where topological invariants distinguish the various phases. In solid materials, the topology of electronic states plays a crucial role in determining their physical properties [1]. For example, the topology of an electronic band is linked to the Berry curvature [2], which has been seen to substantially affect the physical properties of the materials [3, 4, 5, 6].

Berry curvature originates from the entanglement of the valence and conduction band, acting like an intrinsic effective magnetic field [1, 7]. The path integral of Berry curvature defines the Berry phase, an extra phase that the electron wave function acquires upon completing the closed path [2, 5, 8, 9]. The classical concept of a geometrical phase was known for many years; for instance, the trajectory of a Foucault pendulum acquires an extra phase θ after one day. In quantum systems, such a geometric phase can lead to many exotic phenomena, such as anomalous Hall effect [3, 4, 5, 6, 10], topological surface states [11], chiral anomaly [12, 13, 14], and many more [15, 16]. Furthermore, the topological invariant Chern number is the integral of the Berry curvature over a closed surface. Like the number of holes that can be used to define the topology of a classical object, the Chern number is one of the topological invariants that characterize a quantum-mechanical electronic system[17].

Traditionally, the properties of the solid were described by its band structure, depending on the spontaneous breaking of underlying crystal symmetries. Conversely, the discovery of the quantized Hall effect in 1980 showed that the properties of the solids were described without involving/breaking any additional symmetries. In this discovery, Hall conductivity changes step-wise when a two-dimensional electron system is subjected to a varying magnetic field. The steps appear at the integer multiplication of the fundamental constants, e^2/h (where e is a charge of the electron and h is Planck's constant) [18]. As a result, for the first time, the quantized Hall conductivity was measured with a precision of 10^{-9} by von Klitzing [19]. Thus, the discovery of the integer quantum Hall effect opens a new paradigm of the topological orders. One of the consequences is that properties of the material become insensitive to a local perturbation, such as scattering from impurities and defects [18, 20, 21].

The discovery of the quantum Hall effect gave birth to the exploration of the quantum phase of matter, a topological insulator [22]. They are characterized by gapless conducting surface states and insulating bulk [22]. The spin of electrons in these surface states is locked to the parallel or anti-parallel momentum, resulting in the dissipationless flow of charge carriers [23]. This can be a promising asset for use in technological applications. Later, topological aspects were also seen in graphene, a 2D material, in which bands linearly dispersed and touched each other at discrete four-folded points known as Dirac points/nodes.

In the topological material, the energy dispersion is analogous to that of a massless particle traveling at the speed of light, where 'c' is replaced with Fermi velocity 'v_F.' Despite the Fermi velocity is approximately $1/1000$ of the speed of light. As a result, electrons in these bands near the nodes are reminiscent of Dirac fermion, which appears as the solution of the Dirac equation of high energy physics [24, 25]. In recent years, a non-trivial topology was predicted to occur in the three-dimensional electronic structure, leading to the discovery of a new class of topological materials.

1.2 Topological semi-metal

The discovery of graphene (Dirac semimetal, DSM) intensified the search for a 3D topological semimetal. In the last decade, enormous effort has been made to add new materials to the class of topological semimetal, understand the fundamental mechanisms, and reveal potential for technological applications. In this direction, the linear band crosses at the points known as the Dirac node, which has four-fold degeneracy, are found in the 3D semimetal known as the Dirac semimetal. The band intersection can also be a line or loop that further classifies the new type of topological semimetal [26, 27]. Another class of topological semimetal is topological Weyl semimetal (WSM), in which the inverted bands linearly disperse and cross at isolated points called Weyl nodes [28, 29]. Electrons in the Weyl semimetal are seen to be a special solution of the Dirac equation for zero rest mass. Weyl Hermann proposed this solution, so the equation is called the Weyl equation (Eq. 1.1) [30], and the fermions which followed this equation are known as Weyl fermions.

$$H = \chi_c \vec{\sigma} \cdot \vec{p}, \tag{1.1}$$

where, $\chi_c = \pm 1$ is the chirality of the Weyl fermion, $\vec{\sigma}$ is Pauli matrices, and $\vec{p}$ momentum of Weyl fermions.

Unfortunately, no fundamental particle has been found to follow the Weyl equation in high-energy physics experiments until now. Although neutrinos were proposed as massless fermions and were supposed to obey the Weyl equation, later, they were found to be massive [31, 32]. In the last decade, the Weyl fermions have been predicted in the condensed matter as low-energy excitations. Ideally, the Weyl fermions are expected to be massless, but their analogous form in a solid state is observed to have a tiny mass compared to electrons in metals. Conversely, a conventional metal or semimetal has a non-relativistic parabolic band in which electrons have finite rest mass.

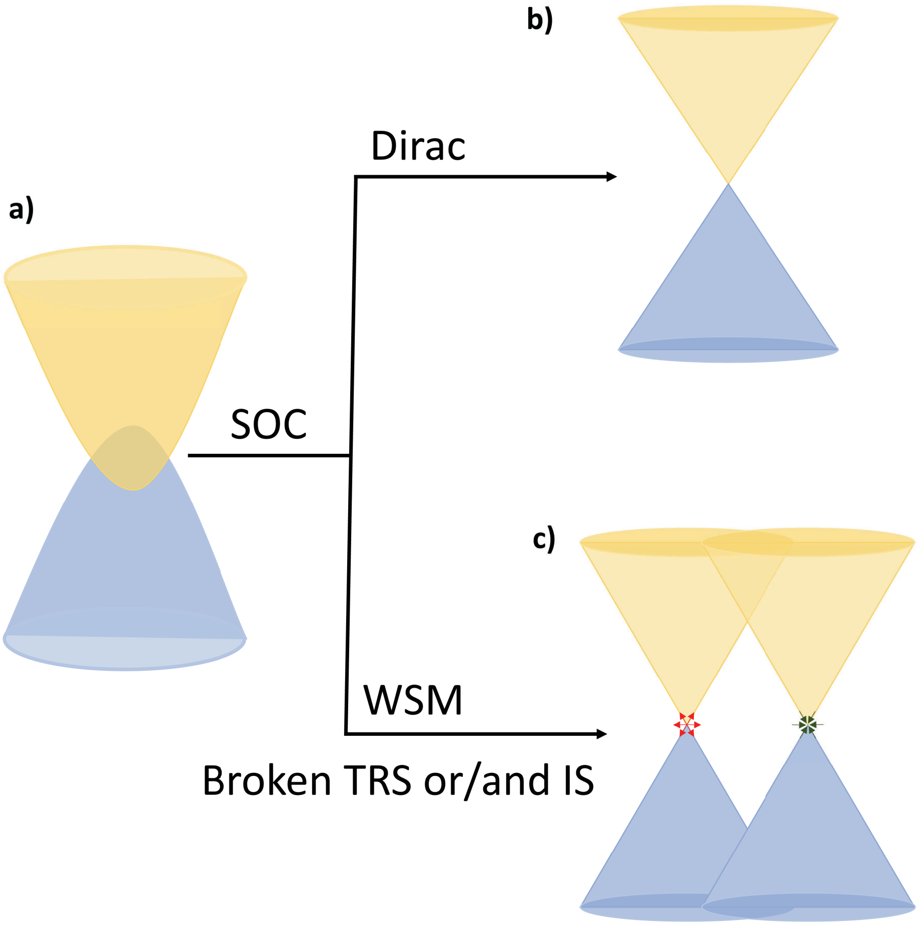

Figure 1.1: a) Band inversion, b) Dirac semimetal- valence and conduction band touch at a point known as Dirac nodes, which has four-fold degeneracy. c) Weyl semimetal (WSM), four-folded degeneracy is lifted by either breaking of time-reversal symmetry (TRS) or/and inversion symmetry (IS). The point of crossing is called Weyl nodes, which come in pairs with a well-defined chirality, i.e., "+" and "-" shown by inward red and outward blue arrows. The nodes are monopoles (source and sink) of Berry curvature.

The four-fold degeneracy of the Dirac nodes can be lifted by breaking inversion symmetry (IS), time-reversal (TR) symmetry, or both. A magnetic field (intrinsic or extrinsic) breaks the TR symmetry, and IS breaks when a crystal does not have a center of inversion. Such lifting of degeneracy leads to the emergence of the Weyl semimetal phase (see Fig. 1.1). Thus, the Weyl semimetal appears to have two copies of a Dirac semimetal. They have different symmetry and physical properties from the Dirac semimetal. For example, the Dirac semimetal respects both TR and IS. In WSM, the spin of electrons is aligned either parallel or anti-parallel with their momentum, which defines the handedness or chirality of electrons in respective nodes. The Weyl nodes come in pairs: a node with one type of chirality and its counter-node with opposite chirality [29].

Weyl nodes are also thought to be magnetic monopoles and anti-monopoles of the Berry curvature [33] with Chern number as topological charges [34, 35]. The Berry flux penetrating the surface that contains a Weyl node can be expressed as $2\pi\chi$ [7, 36]. The sum of the Chern numbers (or topological charge) for the Weyl pair over the entire Brillouin zone must be zero. The Weyl pairs are topologically stable if they are well separated in momentum space [37]. Distinct chirality of the Weyl nodes makes a Weyl semimetal different from a Dirac semimetal, and therefore, chirality-related properties are exclusively visible in WSM.

For example, the projection of bulk Weyl nodes of opposite chirality appears to be connected via chiral gapless edge states, also known as surface Fermi arc [16, 35, 38, 39, 40, 41]. However, double Fermi arcs are seen on Dirac semimetals [35, 42, 43], which are differently topologically protected than Weyl semimetals [36]. These surface states can offer a dissipationless path for Weyl fermions and have been indirectly probed by quantum oscillations [44].

Weyl semimetal types: A form of band intersection determines the kind of a Weyl semimetal. For instance, if bands intersect at isolated points, resulting in a point-like Fermi surface, the emerging phase is a type-I Weyl semimetal (see Fig. 1.2a). Similarly, when the Weyl points appear from the touching of an electron and hole pockets, the Weyl semimetal is classified as type-II. These Weyl semimetals have tilted Weyl cones (see Fig. 1.2b) and open Fermi surface. The Weyl semimetal of type-II shows somewhat different physical properties in comparison with the type-I WSM because the former does not respect the Lorentz symmetry [45].

For example, the chiral anomaly can occur along any crystallographic direction when a type-I WSM is subjected to the parallel electric and magnetic field. However, this is not the case in type-II WSM due to the tilted Weyl cones in energy-momentum space, and it requires a larger kinetic component of dispersion energy than the potential component for a sizable effect of chiral anomaly [45].

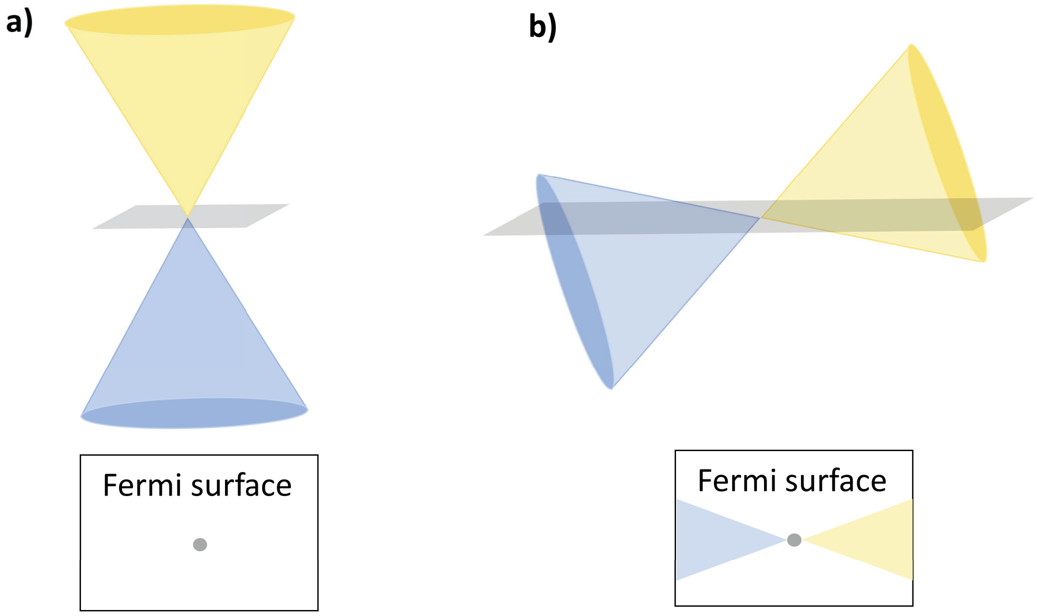

Figure 1.2: a) Type-I and b) type-II Weyl semimetal with Fermi surface shown below, respectively.

Magnetic Weyl semimetal: The Weyl semimetals, in which time-reversal symmetry is broken due to a magnetic ordering, are known as magnetic Weyl semimetals. Magnetic WSMs provide a promising platform for studying the interplay between magnetism and the topology of electronic band structure. Due to the magnetic order, these materials offer a unique opportunity to explore the effects of magnetization. For example, depending on the direction of magnetization, one can create or annihilate Weyl points and shift their position in momentum space. Therefore, it may often result in the tuning of the band structure along with Berry curvature [46, 47, 48, 49, 50, 51]. The effects associated with Berry curvature in magnetic Weyl semimetals are significant, resulting in large anomalous Hall [52, 49, 50], thermoelectric responses [51], and other quantum effects [53, 54]. In some magnetic Weyl semimetal, the topological Hall effect was observed, originating from real-space Berry curvature associated with non-trivial spin structure [55, 56]. However, a strong magnetocrystalline anisotropy can prevent the formation of spiral order [57], resulting in no topological Hall effect. Magnetic Weyl semimetals such as GdPtBi [58, 59], NdAlSi [57], and many more, hold great promise for a variety of quantum phenomena, such as chiral anomaly, gravitational anomaly, and non-trivial features in magnonic [60] and phononic band structures [61]. On the other hand, the topology of the electronic band structure can also play a critical role in magnetic ordering; for example, helical magnetism has been reported to be mediated by Weyl fermions [57].

In summary, Weyl fermions predicted and evidenced to exhibit various anomalous phenomena. Additionally, the Weyl semimetal provides a platform for testing the quantum anomalies proposed in high-energy physics. These quantum anomalies may pave the way for understanding the standard model of particle physics based on quantum field theories.

1.3 Electrical transport of Weyl semimetal

Transport measurements play a vital role in elucidating the exotic effects of quantum materials. Their studies provide the opportunity for a better understanding of the quantum mechanical behavior of carriers near the Fermi level. Transport measurements have a resolution of several meV, making them valuable techniques in search of low-energy excitation, which is especially expected in Weyl semimetal systems. The electrical transport coefficients, such as electrical conductivity, the electronic contribution to thermal conductivity, and magneto-resistance, can be derived by solving the Boltzmann equation [62, 63]. Moreover, one can manifest the Berry curvature effects in the transport coefficients. The chiral anomaly can be manifested as positive magneto-electrical conductivity, i.e., chiral magnetic effect. Additionally, the cyclotron motion of Weyl fermions, as low-energy, non-trivial topological excitations, can be realized through quantum oscillations.

1.3.1 High magneto-resistance (MR)

Weyl semimetals have been predicted to show many exotic phenomena affecting, among others, electrical and thermal conductivity. The variation of resistance in the presence of a magnetic field (B) is referred to as magneto-resistance (MR) and is expressed as:

$$\text{MR} = \frac{\rho(B) - \rho(0)}{\rho(0)}, \tag{1.2}$$

where $\rho(0)$ and $\rho(B)$ are resistivity in zero and magnetic field, respectively.

In conventional metal, MR increases with the magnetic field due to the Lorentz effect and eventually saturates at a sufficiently large magnetic field ($uB \gg 1$, where u is mobility) when the Fermi surface is closed. In the case of an open orbit, the MR does not saturate. Therefore, MR measurements can also be employed to investigate whether the Fermi surface is closed or open [64]. In semimetal, a significant non-saturating MR was also attributed to compensation of charge carriers, i.e., an equal number of electrons and holes. The MR in semimetal increases as B^2 [65]. Conversely, large linear MR has been linked to the topological nature of the material [66, 67]. A giant non-saturating MR has been reported in the topological semimetals [68, 69, 70]. One may consider this to be a characteristic of Weyl semimetal. Weyl fermions are protected from backscattering and can result in a transport lifetime longer than the quantum lifetime. The lifting of this protection by magnetic field leads to a very large MR [68]. In these materials, MR also reminds so-called "quantum linear MR," which emerged when only the chiral lowest Landau level crosses the Fermi level [71].

Moreover, the quantum linear MR appears when quantized Landau levels become well-separated, meaning there is no thermal broadening or smearing of charge carriers between them, i.e., $\hbar\omega_c >> k_B T$ and $\omega_c \tau > 1$, where ω_c is cyclotron frequency, $\hbar$ is reduced Planck's constant, τ is relaxation time, k_B is Boltzmann constant, and T is temperature. Additionally, the Weyl semimetal hosts low-energy excitations with low effective mass due to linear band structure, resulting in large Fermi velocities ($\nu_F = \frac{\hbar k_F}{m^*}$, where k_F is Fermi wavevector and m^* is effective mass). The low effective mass, large Fermi velocity, and large relaxation time [68] of these low-energy topological excitations result in extremely high mobility (the mobility in Dirac dispersion $u = \frac{e\nu_F \tau}{\hbar k_F}$) [65, 70]. The material with ultra-high mobility appeared to have large MR non-saturating at sufficient large magnetic field [64].

1.3.2 Quantum oscillation

In a magnetic field, the 3D bands are quantized into Landau levels, or the allowed energy states lie on Landau tubes formed in k-space (shown in Fig. 1.3). For conventional parabolic bands, the energy eigenvalue of the quantized energy state is given as (Landau's solution for the Schrodinger equation in a magnetic field):

$$\epsilon = \left(n + \frac{1}{2}\right)\hbar\omega_c + \frac{\hbar^2 k_z^2}{2m^*}, \tag{1.3}$$

where n is the Landau level index, $\omega_c = \frac{eB}{m^*}$. Here, B is the applied magnetic field along the z-direction (or the axis of concentric circular cylindrical tubes).

Under such conditions, the motion of a fermionic quasiparticle is constrained to the quantized Landau orbits. These quantized landau levels separate equally when subjected to the magnetic field (Eq. 1.3), i.e., $\hbar\omega_c$.

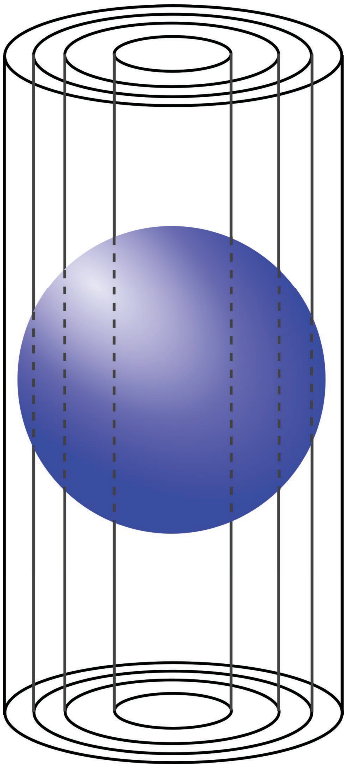

Figure 1.3: Schematic of Landau tubes, where the solid-blue sphere represents Fermi surface in zero magnetic field. With increasing the magnetic field (applied along the axis of the Landau tubes), the tubes expand and cross the Fermi level. This results in oscillation of the electronic density of states and related physical properties like electrical conductivity, magnetization, and thermal conductivity.

The Landau tubes start to expand with increasing B, and each time, they cross the Fermi level, giving rise to a peak in the density of the electronic states. This results in quantum oscillations that are periodic in $1/B$. The frequency of the oscillation can be related to the extreme cross-sectional area of the Fermi surface given by the Onsager relation:

$$F = \frac{\hbar}{2\pi e}A, \tag{1.4}$$

where F is the frequency, and $A = \pi k_F^2$ is the extreme area of the cross-section (assuming the Fermi surface has a spherical shape).

The quantum oscillations can appear in many physical properties [72]. For example, the oscillation observed in resistivity is known as the Shubnikov-de Haas (SdH) effect [73]. There are two conditions for realizing the quantum oscillation in conducting solid materials. First, the Landau level's thermal broadening should be smaller than the distance between them; $k_BT < \hbar\omega_c$. This condition is usually satisfied at low temperatures and in high B fields. Accordingly, the amplitude of quantum oscillation diminishes with increasing temperature due to blurring out the boundary of occupied and unoccupied states.

The second condition is that the broadening of the Landau level due to interaction with impurities/defects should be smaller than the separation between the levels; $\hbar/\tau < \hbar\omega_c$ or $\omega_c\tau > 1$, known as the clean limit of a material, meaning that the charge carriers complete a closed revolution without being scattered. Such condition can be fulfilled in single crystals with few impurities or defects, i.e., high-purity single crystals.

However, in the case of relativistic fermions (Weyl semimetals), the Landau levels are no longer equally spaced as Weyl semimetals have linear bands. Therefore, their eigenvalues are given as [74, 75]:

$$E(n) = \nu_F \sin(n)\sqrt{2\hbar Ben}. \tag{1.5}$$

For the 3D relativistic fermions, an additional term appears due to unquantized Landau levels along the direction of the applied magnetic field in the above Eq. 1.5 [76]:

$$E(n) = \nu_F \sin(n)\sqrt{2\hbar Ben + (\hbar k_z)^2}. \tag{1.6}$$

Generally, Weyl semimetals have small Fermi surfaces, so one can anticipate frequencies with small cyclotron masses and non-trivial Berry phases that can be calculated from quantum oscillation analysis. One can reconstruct the topology of the Fermi surface by probing its extreme cross-section area perpendicular to the magnetic field using quantum oscillations. One of the predominant characteristics of Weyl semimetal is the surface Fermi arcs. The arcs connect the projection of two Weyl points of opposite chirality on two opposite surfaces (top and bottom) of the sample, forming closed orbits passing through bulk chiral states called Weyl orbits. As a result, the cyclotron motion of Weyl fermions can be observed through quantum oscillation. However, the oscillation associated with the Weyl orbits is limited to thin layers of Weyl semimetal. In such a case, the thickness of the layer has to be smaller than the mean free path of the electron. Noteworthy, an ideal Weyl semimetal, in which the Fermi level is tuned to the location of the Weyl node, does not show any quantum oscillation.

1.3.3 Chiral anomaly

Quantum field theory (QFT) describes the chiral anomaly as the creation and annihilation of a relativistic particle with well-defined chirality from the vacuum state. The vacuum state is defined as the Dirac sea of negatively occupied energy states at zero temperature and chemical potential. In condensed matter, the vacuum state refers to the occupied electronic states below the Fermi surface, which is finite. However, anomalies can also occur in real systems at finite chemical potential and temperatures, as described in a recent review by *Chernodub et al.* [77].

In QFT, the parallel configuration of electric (**E**) and magnetic fields breaks the law of chirality conservation, which is a classically conserved quantity. The law states that a system has an equal number of particles with one chirality to its counterparts. The breakdown of the chiral conservation law at the quantum level is a macroscopic manifestation of chiral anomaly, also known as the Adler-Bell-Jackiw (ABJ) anomaly.

In high-energy physics, the state with negative energy is never realized experimentally. However, in condensed matter physics, the electronic states below the Fermi level are considered negative energy states. This motivates the condensed matter physics community to realize the chiral anomaly in solid materials via experiments/theory.

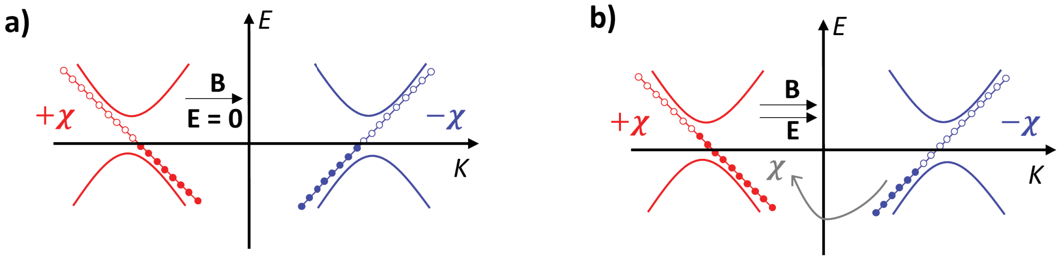

Figure 1.4: a) Equally populated chiral Landau level with chirality $\chi = \pm 1$, blue with negative chirality, and red with positive chirality, in the presence of the magnetic field. b) An application of parallel electric and magnetic fields leads to a higher number of Weyl fermions at a positive chirality Landau level (red) than at a negative chirality Landau level (blue). Such imbalance in the population of Weyl fermions between the Weyl nodes of opposite chirality breaks the conservation law of chirality, and this phenomenon is called a chiral anomaly.

In the case of Weyl semimetal (or DSM in a magnetic field), one chirality Weyl fermions are created. In contrast, the opposite chirality is annihilated in respective Weyl nodes when subjected to parallel B and **E**. In other words, an imbalance in the population of two opposite chirality Weyl fermions occurs within a pair of Weyl nodes in the presence of parallel B and **E**, leading to the violation of chirality conservation law [14, 78]. As a result, the charge pumping between Weyl nodes of opposite chirality occurs, and an additional electric current starts flowing. This phenomenon is known as the chiral magnetic effect and can be observed as negative longitudinal magnetoresistance (NLMR)/ positive magnetoelectrical conductivity. In high-energy physics, the analogous current is called axial current [79], relaxed by the inter-valley scattering events [80, 81].

In case of chiral anomaly, the hierarchy of scattering time can be understood as $\tau < \tau_{inter} < \tau_{e-e} < \tau_{e-ph}$, where τ is intra-valley, τ_{inter} is inter-valley, τ_{e-e} is electron-electron, and τ_{e-ph} is electron-phonon scatterings. In intra-valley scattering, Weyl fermions are rapidly scattered with each other within the same chirality Weyl nodes, leading to a slight change in momentum. As a result, the Weyl fermions remain in the same chirality Weyl nodes. However, in the case of inter-valley scattering, one chirality, Weyl fermion, jumps from one node to another, resulting in a significant momentum exchange.

Furthermore, electron-electron and electron-phonon interactions are assumed to be minimal compared to the inter-valley scattering process. It leads to a an ideal situation where $\tau = 0$ and $\tau_{e-e}, \tau_{e-ph} \approx \infty$. The chiral magnetic effect shows unique field dependency based on the strength of the external magnetic field and the position of the Fermi level from the Weyl nodes. In the semi-classical regime, when chemical potential (μ) is much larger than thermal excitation energy, and in the low-field regime, the chiral anomaly contribution to electrical conductivity, σ_{chiral}, is given [80, 82]:

$$\sigma_{\text{chiral}} = \frac{N_{wp} e^2}{8\pi^2 \hbar} \frac{(eB)^2}{\epsilon_f^2} v_F^3 \tau_{\text{inter}}, \tag{1.7}$$

where:

N_{wp} : is the number of Weyl points/nodes,

ϵ_F : is the Fermi energy.

In a high field regime or the quantum limit (when only the lowest Landau level remains populated), $\sigma_{chiral}(B)$ shows linear magnetic field dependency [83]. In the quantum limit of the material, one can anticipate the maximum contribution of the chiral magnetic effect [84]. However, in some Weyl semimetals, the quantum limit might be attained at an exceptionally high magnetic field, which can be experimentally challenging.

However, special care has to be taken while performing electrical transport experiments to observe the chiral magnetic effect. For example, the classical extrinsic artifacts, such as the current jetting effect [85], can make it obscure to observe and interpret. With increasing the magnetic field, the current jetting effect induces an inhomogeneous current flow across the sample, resulting in higher voltage at one pair of contacts while small or even zero voltage at the other one [85]. The current jetting effect is expected to be significant in samples with highly mobile carriers and large anisotropy in electrical conductivity. Therefore, in samples with high mobility and point-current contacts, the positive magneto-conductivity or negative magneto-resistance can also caused by the current jetting effect [86, 87]. Using/measurements of the sample with moderate/reduced mobility and cross-sectional-current contact can reduce the risk of such detrimental effects.

1.4 Thermal transport

In solid conducting materials, electrons carry charge and energy when subjected to a temperature gradient. Similar to the electrical response of a sample to an externally applied voltage, the response of the sample to thermal stimuli can also provide valuable information about the system. This knowledge might be not only complementary to that inferred from other measurements but, to some extent, irreplaceable. The thermal phenomena also appear less susceptible to various detrimental effects, which may make the electrical transport results challenging to interpret. For example, the current jetting does not affect thermal conductivity as no external electrical voltage is applied; instead, heat is supplied. Consequently, it can be a source of remarkable insight, especially about the chiral anomaly in Weyl semimetals [1, 77, 88]. The thermal transport measurements are extremely useful in the study of charge-neutral excitations. Furthermore, these measurements can also be used to test anomalies predicted by the QFT for chiral fermions.

In this thesis, we present collective topological excitations that have been observed in Weyl semimetal. Namely, the chiral zero sound (CZS) and the gravitational anomaly effect of Weyl fermions were experimentally realized in the collinear magnetic field and temperature gradient.

1.4.1 Thermal conductivity

Thermal conductivity (κ) is the ability of a matter to conduct heat from the hot side to the cold side. It plays a central role in a vast number of applications, including isolation, heat transfer, batteries and capacitors, and many more. Therefore, its understanding and measuring methods are quite crucial from a practical point of view. In matter, heat propagates through convection, radiation, and conduction. However, in solids, heat conduction is the dominant mechanism, which is expressed using Fouriers Law [89]:

$$Q = -\kappa \nabla T, \tag{1.8}$$

where Q is heat flux passing through the unit cross-section area per unit time, and ∇T is temperature gradient.

According to the kinetic theory of thermal transport, the general formula for thermal conductivity in d-dimensional space is given by [90]:

$$\kappa = \frac{1}{d(2\pi)^d} \int C_k \cdot v_k \cdot l_k \; dk, \tag{1.9}$$

where C_k is the contribution to the total specific heat at constant pressure (in solid), v_k is velocity, and l_k is the relaxation length of the k^{th} mode.

Above equation (Eq. 1.9) can be further simplified for 3D [91]:

$$\kappa = \frac{1}{3} C v l, \tag{1.10}$$

where:

C : Specific heat capacity at constant pressure (in solid),

v : Average velocity of the (quasi)particles,

l : Mean free path of the (quasi)particles.

In materials, heat is carried by electrons, phonons, magnons, and topological excitations, depending on their respective band structure (electronic and magnonic) and involved scattering mechanisms. For instance, magnons might be the dominant heat carriers in magnetic materials and can significantly scatter phonons. This scattering mechanism substantially attenuates the phonon contribution to thermal conductivity [92].

In conducting non-magnetic materials, electrons and phonons effectively carry heat, and their impact as dominant heat carriers depends on various factors, including temperature range and scattering mechanisms. For example, at low temperatures, the phonon mean free path is limited by sample dimensions in a pure crystal. In contrast, their mean free path can be limited by the crystallographic defects in an imperfect crystal. Nevertheless, in both cases, the mean free path is temperature-independent. At higher temperatures, the anharmonic motion of the lattice can substantially enhance phonon-phonon scattering, resulting in significant suppression of phonon contribution to κ.

On the other hand, electronic contribution to κ usually dominates the thermal transport at all temperatures in metals. However, the collision of electrons with impurities and lattice disorders can limit the electronic contribution in impure metals. In such cases, the lattice contribution may become comparable to the electronic contribution.

To stay within the scope of this thesis, we will limit our discussion of thermal conductivity to the Weyl semimetals. In Weyl semimetals, topological excitations can also carry heat along with electrons and phonons. Additionally, magnons can also participate in heat transport in a magnetic Weyl semimetal. According to Matthiessen's approximation, which states the relaxation time of different scattering events is additive, the total thermal conductivity in a magnetic Weyl semimetal can be expressed as the sum of possible individual contributions:

$$\kappa_{\text{total}} = \kappa_{el} + \kappa_{ph} + \kappa_{m} + \kappa_{excitaion}, \tag{1.11}$$

where κ_e, κ_{ph}, κ_m, and $\kappa_{excitaion}$ are electronic, lattice, magnonic thermal conductivity and other excitation contributions to κ, respectively.

The qualitative influence of lattice and magnon contributions to thermal conductivity is to be discussed in the coming sub-sections. In compensated semimetals, a bipolar contribution that can emerge from the recombination of electrons and holes at the cold end of the sample should also be considered.

1.4.1.1 Electronic thermal conductivity

In conducting solid, electronic contribution in total thermal conductivity by Boltzmann equation [62]:

$$\kappa_e = \frac{1}{4\pi}\int \tau\vec{v}\vec{v}\epsilon_f^2\frac{\delta f_0}{\delta\epsilon}d^3k, \tag{1.12}$$

taking the integration over Fermi surface (FS):

$$\int_{\mathrm{FS}} d^3k = \int d^2S\, dk_\perp = \int_{FS} d^2S dE/|\delta E/\delta\vec{k}| = d^2S dE/(\hbar v).$$

Using the δ-function property of $(\delta f_0/\delta E)$ above equation can be simplified:

$$\kappa_e = \frac{(k_BT)^2}{12\pi\hbar}\int \tau\vec{v}\vec{v}\frac{d^2S_{FS}}{v}. \tag{1.13}$$

It is known that electrical conductivity from the Boltzmann equation;

$$\sigma = \frac{e^2}{4\pi\hbar}\int \tau\vec{v}\vec{v}\frac{d^2S_{FS}}{v}.$$

Electrical thermal conductivity in Eq. 1.13 becomes;

$$\kappa_e = \sigma T\frac{\pi^2k_B^2}{3e^2}. \tag{1.14}$$

The above equation (Eq. 1.14) is known as the Wiedemann-Franz (WF) law that links heat and charge transport coefficients, i.e., electrical thermal conductivity and electrical conductivity. One can quantify the electronic thermal conductivity using the WF law.

$$L = \frac{\kappa_e}{\sigma T}(\frac{e}{k_B})^2, \tag{1.15}$$

where L is known as the Lorenz number.

For the Fermi liquid, L is equal to the Sommerfeld value L_0 =2.44 $\times 10^{-8}$ $\mathrm{V^2K^{-2}}$ in the elastic scattering regime of conduction electron. An elastic scattering equally affects the charge and heat current. Usually, the WF law is obeyed at low and high temperatures (with reference to Debye temperature) in metallic systems. However, small wavelength phonon scattering at intermediate temperatures is considered inelastic and significantly influences the transport of carriers. For instance, small-angle electron-phonon scatterings are expected to significantly affect heat transport while the charge current remains insensitive to the scattering. As a result, L is lower than L_0 [93].

1.4.1.2 Ambipolar contribution to thermal conductivity

In a semimetal with multiple electron and hole pockets, there is a possibility of recombination of electrons and holes during the diffusion event. The creation-annihilation process results in the emergence of a charge-neutral heat transfer channel that can carry heat [94, 95]. This additional contribution is known as an ambipolar or bipolar contribution. In Weyl semimetal, the ambipolar contribution to the thermal conductivity (κ_{e-h}) can be expressed as [96, 97]:

$$\kappa_{\text{e-h}} = \frac{\pi^4 k_B^2}{9e^2} T \left(\frac{\sigma_e \sigma_h}{\sigma_e + \sigma_h} \right) \left(\frac{k_B T}{E_F^e} + \frac{k_B T}{E_F^h} \right)^2, \tag{1.16}$$

where E_F^e and E_F^h represent the Fermi energy of electrons and holes, respectively. σ_e and σ_h denote the electrical conductivity associated with electrons and holes.

On the other hand, κ_{e-h} becomes negligible for $T \ll T_F$ (where T_F is the Fermi temperature) [98]. Furthermore, for a significant κ_{e-h}, the electron and hole pockets have to be in close proximity in the momentum space, and their respective contributions to the thermal conductivity should be comparable.

1.4.1.3 Lattice thermal conductivity

In the crystalline solid, the displacement of atoms from the nominal equilibrium position results in elastic sound waves, which are referred to as crystal lattice vibrations. The quantized lattice vibrations are known as phonons, with energy $\hbar\omega$ and a pseudo-momentum $\hbar k$. Therefore, the macroscopic consequences of phonons dynamics can be seen in the physical properties of a solid, such as electrical conductivity, thermoelectric power, specific heat, and thermal conductivity. When a solid is subjected to a temperature gradient, phonons also carry heat from the hot side to the cold side. Their movement is relaxed by grain boundaries, impurities, electrons, and other phonons. Thus, the relaxation/scattering mechanisms decide the extent to which they contribute to thermal conductivity.

In insulating solids, phonons themself substantially contribute to thermal transport, serving as dominant heat carriers to κ. However, quantifying the lattice contribution is challenging in metallic or semi-metallic systems. One can calculate the upper limit of lattice thermal conductivity (Eq. 1.10), assuming that the mean free path of phonon is limited by the sample physical boundary. The qualitative impact of phonons on thermal conductivity (using Eq. 1.10) is briefly discussed in different temperature regimes, which depends on the scattering mechanisms involved [94, 99].

1. High temperatures ($T \gg \Theta$, where Θ is Debye temperature): In this temperature range, the specific heat saturates, and Umklapp scattering processes are the main limiting factor for $\kappa_p h$. Assuming sound velocity is constant, κ_{ph} can be written as,

$$\kappa_{ph} \propto \frac{1}{T} \quad \text{and} \quad l \propto \frac{1}{T}.$$

2. Intermediate temperatures ($T < \Theta$): In this temperature range, which is known as the "Ziman regime [100]," the Umklapp process is significant at the beginning temperatures of the region. However, as the temperature decreases, these scattering processes become less frequent, while normal collisions of phonons become more frequent. Notably, the normal collision of phonons doesn't contribute to thermal resistance. The scattering of phonons with lattice disorder or impurities starts to limit their mean free path.

$$l \propto \exp\left(\frac{\alpha\Theta}{T}\right)$$

where α is a constant parameter.

In this temperature range, the specific heat is proportional to T^3. Thus, assuming the sound velocity is constant, κ_{ph} has the form:

$$\kappa_{ph} \propto T^3 \exp\left(\frac{\alpha\Theta}{T}\right).$$

The cooling can affect the thermal conductivity via a decrease in phonon density and an increase in the scattering time. Both effects cancel each other impact on thermal conductivity, resulting in a peak to κ_{ph}.

3. Low temperature ($T \ll \Theta$): At low temperatures, the mean free path is limited by the sample boundary; therefore, it is temperature-independent.

$$\kappa_{ph} \propto T^3 \quad ; \quad C_{ph} \propto T^3.$$

However, in imperfect crystal, the above dependency is expected in the winder temperature range, and the phonon mean free path is limited by disorders or impurities [94].

4. Hydrodynamic window: The window lies between the low-temperature regime and the peak that appeared in the thermal conductivity (see Fig.2c in [101]). The phonon mean free path in this temperature range is not limited by sample size. The normal phonon-phonon collision is more frequent than the Umklapp phonon-phonon scattering. In a hydrodynamic window, the lattice thermal conductivity increases faster than T^3 [101].

Magnetic field dependence of lattice thermal conductivity: Phonons are considered insensitive to magnetic fields because they are chargeless and have no magnetic moment. However, there are instances where phonons are seen to be coupled with magnetic field [102, 103]. Among them, one phenomenon is the anharmonic motion of lattice in a magnetic field, leading to an impactful phonon-phonon scattering. As a result, lattice thermal conductivity is reduced [104]. Another mechanism is field-dependent phonon scattering over the multiple energy states of free or paramagnetic spins. The magnetic field lifts the degeneracy of the energy state and can lead to the two levels of Schottky anomaly. This anomaly is expected to appear in the specific heat. The scattering mechanism associated with it affects the thermal conductivity [105, 106]. Additionally, in magnetically ordered materials, resonant scattering of phonons due to magnons attenuates their contribution to thermal conductivity [92]. This resonance scattering is believed to be reduced with a magnetic field. As a result, the thermal conductivity increases [107, 108].

1.4.1.4 Magnonic thermal conductivity

In the case of magnetic samples, spin vibration caused by thermal energy may result in collective magnetic excitations. Quantized magnetic excitations are known as magnons, similar to phonons, which are quantized lattice excitations. Magnons carry energy and momentum, marking their characteristics into physical properties, especially heat capacity, magnetization, and thermal conductivity. Like acoustic phonons, acoustic magnon branches substantially contributed to heat transport because they have non-zero group velocities. While the non-dispersive magnons have zero group velocity, they can act as a scatter for acoustic magnons and phonons.

However, the impact of magnons on thermal conductivity depends on the involved scattering mechanisms or relaxation processes. The thermal conductivity of the magnons is given by the kinetic expression Eq. 1.10. The quantification of magnon thermal conductivity can be challenging due to the interaction of the magnons with other quasi-particles, defects, and grain boundaries. However, one can qualitatively estimate the magnon thermal conductivity, assuming the magnon mean free path is limited by the size of the crystal and constant group velocity. Therefore, at low temperatures, magnon thermal conductivity exhibits the same temperature dependency as specific heat. The specific heat is calculated using the energy-momentum dispersion relation and density of the states of magnons (given by the Bose-Einstein distribution function). The dispersion relation might be distinct for different types of magnetic material. For example, the magnons in simple antiferromagnetic material, referred to as antiferromagnetic magnons, have a linear dispersion relation, while the magnons in ferromagnetic show a quadratic dispersion relation [109].

In magnetic materials, the magnetic spin excitations occur below the magnetic transition temperature. It was reported that magnons substantially carry heat in magnetically ordered solids [110, 111]. It has also been observed that magnons contributed effectively to heat transport, resulting in an equal or greater heat capacity and thermal conductivity than those of phonons [112]. Their effect on total thermal conductivity can be seen as a deviation from a purely phononic T^3 behavior when phonon transport is limited by the sample dimensional at low temperatures [113, 114]. For extracting the magnon thermal conductivity experimentally, phonon and electron contribution to thermal conductivity should be estimated and subtracted from experimental total thermal conductivity, i.e., $\kappa_m = \kappa_{total} - \kappa_e - \kappa_{ph}$.

In this regard, the phononic thermal conductivity can be estimated in two ways. In the first approach, the phononic thermal conductivity is calculated using the specific heat capacity of sister non-magnetic material. Firstly, the specific heat of the sister material was fitted with $aT + bT^3$, where aT is the electronic contribution and bT^3 is the phononic contribution to heat capacity in a low-temperature regime (above the magnetic transition temperature). Subsequently, the extracted phononic contribution was scaled to match the remaining non-electronic thermal conductivity of the target material [106]. In the second approach, the lattice thermal conductivity was obtained, assuming the magnonic contribution can be exponentially suppressed with B [115, 116]. At a sufficiently high magnetic field, thermal conductivity saturates to lattice thermal conductivity, assuming that the phonon is chargeless, has no magnetic moment, and barely interacts with a magnetic field.

In the magnetic field, magnons carry heat in either themselves or by hybridizing with phonons [117]. In the former, if a sufficiently large magnetic field is applied, a gap can be created in the density of state for magnons [118]. When the gap (minimum energy required for the magnons to propagate) is less than the Zeeman energy, it leads to the freeze-out of magnons in the specific heat capacity and thermal conductivity. Consequently, their contribution to total thermal conductivity decreases exponentially with the magnetic field. Therefore, in a high magnetic field regime, magnons carry negligible or even no heat when the thermal activation energy is much smaller than the gap energy.

1.5 Collective topological excitations

Weyl semimetals provide a playground for searching for low-energy topological excitations. Some are charge-neutral, requiring a robust technique other than electrical transport to observe their experimental signatures. Since collective excitations can often be associated with heat transfer, thermal conductivity can be used to study their properties. These excitations can serve as additional or anomalous heat channels. For example, an additional heat channel can be formed by chiral zero sound [119, 120, 121]. Another topological excitation has resulted from the relativistic Weyl fermions in heat transport, known as gravitation anomaly when a Weyl semimetal is subject to the parallel magnetic field and temperature gradient. It results in an anomalous contribution to thermal conductivity [1, 77, 88, 122, 123, 124, 106]. In this thesis, heat conduction mechanism due to chiral zero sound and gravitational anomaly has been observed in Weyl semimetal NbP and NdAlSi, respectively.

1.5.1 Chiral-zero sound

Landau's theory of Fermi liquid proposed the concept of quasiparticles and various collective sound modes propagating under specific circumstances in the vicinity of the Fermi level. Ordinary sound propagates through the medium in the form of dynamic compression and rarefaction. As the effect is mediated by collisions, the sound propagation is prohibited in the collisionless regime (i.e., $\omega\tau >> 1$ where ω is the frequency and τ is collision time), usually expected at low temperatures. Under the collisionless limit, local density increases, and the interaction among quasiparticles can drive the neighboring quasiparticle through modification of the effective field, which acts as a restoring force between quasiparticles [125]. Such restoring force changes the character of sound propagation, and a new kind of sound can emerge called zero sound [126, 127, 128, 129, 130], which is a manifestation of the breathing modes of the Fermi surface. The phenomenon was first observed in liquid He^3 [127]. In ordinary metallic systems, electronic states have a gap, the so-called plasmonic gap, due to long-range Coulomb interaction. This gap makes it difficult for electrons to produce sound waves. The existence of zero sound modes requires strong and anisotropic residual interactions. Usually, such conditions are not satisfied in normal metals.

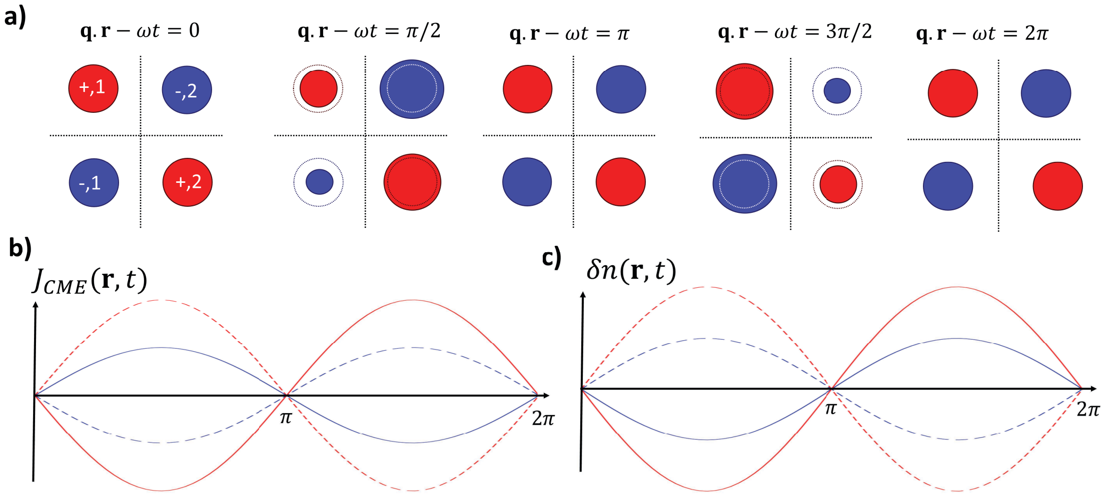

Figure 1.5: Chiral zero sound (CZS) modes in two pairs of Weyl points, red and blue, with negative and positive chirality. a) The Fermi surface is represented by disks around the Weyl points, and the equilibrium position of the Fermi surface is depicted by dashed circles. The Fermi surface of one chirality Weyl point oscillates in an out-of-phase manner, resulting in complete charge cancellation. b) The chiral magnetic effect contribution from subvalley 1 and 2 with positive (negative) chirality is shown in red (blue) solid and dashed curves, respectively. c) Net density of Weyl fermions vanishes from the same chirality subvalleys. The schematics are adapted from reference [120].

In the case of Weyl semimetal, Weyl fermions show a chiral magnetic effect and electronic excitation near the Weyl nodes acting differently than electrons in the metal. In Weyl semimetals with multiple pairs of Weyl points, there is a possibility of an acoustic collective mode called chiral zero sound emerging from the density oscillation in the Weyl valley. More specifically, the same chirality Weyl valleys oscillate in antiphase while the opposite chirality valleys oscillate in phase. Hence, the chiral zero sound modes are completely decoupled from charge dynamics. These modes appear under the chiral limit $\frac{\tau_0}{\tau_s} << 1$, where τ_0 and τ_s refer to intra-valley and inter-valley scattering times, respectively [120]. The CZS mode relies on chiral plasmonic excitations propagating in the antiphase, which leads to the complete cancellation of charge current (see Fig. 1.5) but allows heat transfer. The velocity of these modes is strongly modulated in the magnetic field. At low temperatures, CZS velocity varies with the magnetic field, linearly in low magnetic regions, oscillating in strong ones. One of their experimental characteristics is huge quantum oscillations in thermal conductivity [119, 120, 121]. The CZS provides an additional pathway for heat conduction, resulting in a drastic violation of the WF law.

It is well known that the velocity of sound depends on the compressibility of the medium. In CZS modes, the compressibility is defined by $\beta(B) = \frac{d\rho}{d\mu}$, where ρ is the density of particles. This compressibility oscillates in a magnetic field and the oscillating part of compressibility is calculated by *Song et al. (2019)* [120]:

$$\frac{\beta^{(1)}}{\beta^{(0)}} = \hbar \frac{\omega_B}{\mu} \frac{\exp\left(-\frac{\pi\mu}{\hbar^2\omega_B^2\tau_0}\right)}{sinch\left(\frac{2\pi^2\mu k_B T}{\hbar^2\omega_B^2}\right)} \cos(-\pi\frac{\mu^2}{\hbar^2\omega_B^2} - \frac{\pi}{4}), \tag{1.17}$$

where, $\omega_B = \nu_F\sqrt{\frac{eB}{\hbar}}$ is magnetic frequency ($\nu_F = \sqrt{\nu_x\nu_y\nu_z}$ is mean Fermi velocity), $sinch(x) = \frac{\sinh(x)}{x}$, and $\tau_0 = \frac{6\pi^2\sigma^{elec}\hbar}{N_{WP}(e^2k_F^2\nu_F)}$ is calculated from Drude model for Weyl semimetal.

Given that, the CZS contribution to total thermal conductivity:

$$\kappa_{CZS}(B) = \tau_s k_B \Lambda^3 \nu_F^2 N_{CZS}\left(\frac{(\hbar\omega)^2}{4\pi^2\mu^2}\left(1 - \frac{\beta^{(1)}}{\beta^{(0)}}\right)\right)^2 F\left(\frac{\hbar\nu_F\Lambda}{k_B T}\frac{(\hbar\omega)^2}{4\pi^2\mu^2}\left(1 - \frac{\beta^{(1)}}{\beta^{(0)}}\right)\right), \tag{1.18}$$

where $F(a) = \frac{1}{a^3}\int_{-a}^{a}\frac{x^2(a^2-x^2)}{32\pi^2\sinh^2(\frac{x}{2})}dx$, τ_s is also the relaxation time for chiral zero sound, threshold wave vector for chiral zero-sound mode $\Lambda = 2k_F(\sqrt{\frac{\nu_x\nu_y}{\nu_z}})$, N_{CZS} is the number of Weyl points that contributing to CZS mode and due to anisotropy in Fermi surface the factor is included $\sqrt{\frac{\nu_x\nu_y}{\nu_z}}$. And μ can be calculated using k_F and ν_F, $\mu = \hbar\nu_F k_F$.

1.5.2 Gravitational anomaly

Like the chiral anomaly, the gravitational anomaly was also proposed in quantum field theory and more recently discovered in condensed matter physics [77, 88, 106]. At the heart of the phenomenon is the fact that the gravitational field and the temperature gradient are interrelated [131]. Namely, it was proposed that temperature is not constant in the curved time-space, which results in a close relation between mass and energy in the relativistic system. Heat propagation in the presence of a temperature gradient can also be considered an anologue of mass movement under the influence of a gravitational field [1].

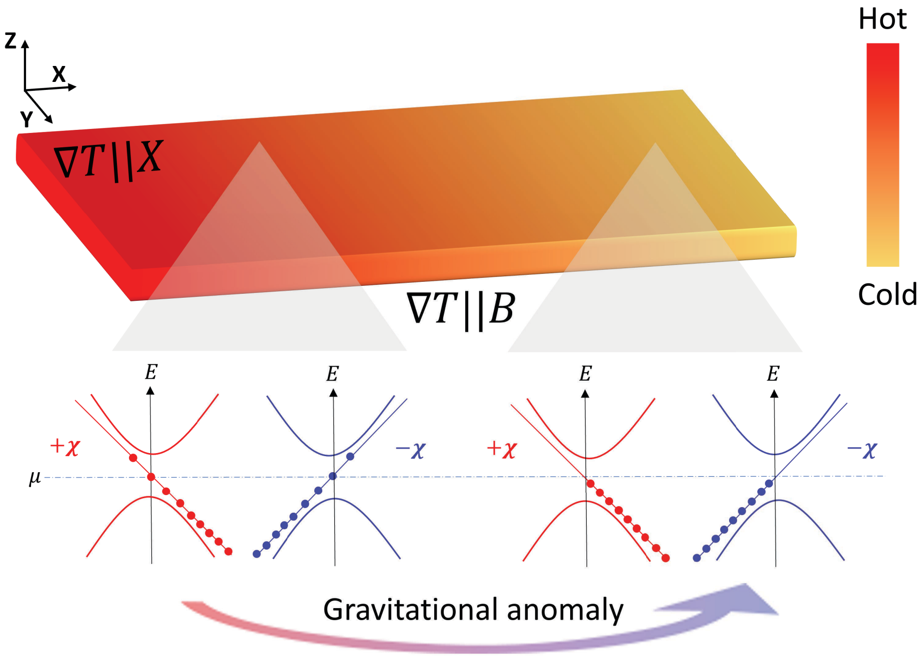

Figure 1.6: Schematic shows an application of temperature gradient to the sample. When a temperature gradient is applied parallel to the magnetic field, temperature imbalance occurs while balancing the numbers of Weyl fermions in respective Weyl nodes. The imbalance is prohibited by the conservation law for energy-momentum tensor, and the phenomenon is called gravitational anomaly.

In Weyl semimetals, an imbalance of temperature (likewise imbalance in chemical potential) can take place between two Weyl points of opposite chirality when the thermal gradient and magnetic field are aligned parallel to each other [1, 77, 88, 106, 132]. This leads to a violation of the conservation law for the energy-momentum tensor [133], which measures the contribution of particle current and heat current to the total energy current. Weyl nodes of opposite chirality are characterized by the same energy-momentum tensors, and thus, they have the same temperature. Such a breakdown of conservation law for energy-momentum tensor is considered as the QFT realization of gravitational anomaly [1, 77, 88, 106, 122, 123, 124].

The solid-state realization of this anomaly results in an anomalous heat current carried by the Weyl fermions while maintaining the same number of Weyl fermions in respective Weyl nodes (see Fig. 1.6). Such anomalous contribution of Weyl fermions can be seen in magneto-thermal conductivity measurements. Further, gravitational-anomaly-related contribution to the longitudinal magneto-thermal conductivity is given [77]:

$$\kappa_{gr} = \frac{\pi^2 k_B^2 \sigma_{ch} T}{3e^2} = L_0 \sigma_{ch} T, \tag{1.19}$$

where L_0 is Sommerfeld value of Lorenz number, σ_{ch} is chiral anomaly contribution to electrical conductivity.

Surprisingly, it can be seen that a classical WF law still holds for these anomalous contributions. Until now, the experimental signature of gravitational anomaly is an increase in magneto-thermal conductivity, which should be proportional to the rise of magneto-electrical conductivity [1, 77, 106, 132].

1.6 Motivation

A Weyl semimetal is a topologically non-trivial material in which valence and conduction bands are inverted and cross each other at isolated points called Weyl nodes. Near the node, the band appears to have linear energy dispersion, leading to the emergence of relativistic-like Weyl bands. The nodes come in pairs with opposite chirality, which are populated by Weyl fermions with parallel or anti-parallel locking of momentum and spin, due to which these materials can have potential applications in electronic devices. Weyl semimetals exhibit many exotic phenomena that are interesting from a fundamental perspective.

For instance, the application of the parallel magnetic and electrical field (or magnetic field and thermal gradient) leads to the pumping of charge (or energy) between the Weyl points of opposite chirality. In the former case, an imbalance of chemical potential, while in the latter, a temperature imbalance occurs between the Weyl nodes of opposite chirality. These two phenomena are considered solid-state realizations of chiral and gravitational anomalies. Another exotic phenomenon in Weyl semimetals with multiple pairs of Weyl points is the possibility of the emergence of an acoustic collective mode called chiral zero sound (CZS). These modes rely on chiral plasmonic excitations propagating in the antiphase, which leads to the complete cancellation of charge current but still allows heat transfer.

In this thesis, we attempted to probe the topological excitations in Weyl semimetals. Preliminary samples of Weyl semimetals were electrically characterized. However, the mentioned excitations of these materials remain elusive for electrical transport. To investigate them, we build a heat transport setup for measuring thermal conductivity. Understanding the mechanism behind the mentioned excitations has the potential not only to deepen our knowledge in the field of topology but also to pave the way for practical applications. This thesis sheds light on their fundamental aspect and attempts to answer questions like:

- Can topological excitations in a Weyl semimetal carry heat but not charge?
- How does the magnetic field influence the properties of topological heat carriers?
- Is the Wiedemann-Franz law obeyed by Weyl fermions?

A group of materials well suited for the investigation of topological thermal properties are Weyl semimetals, which possess not only topological surface states but also non-trivial bulk electronic structure. For the study, we have chosen NbP, which has multiple pairs of Weyl points, and NdAlSi, a magnetic Weyl semi-metal with broken time-reversal and inversion symmetry. NdAlSi also has multiple pairs of Weyl points in its different magnetic phases, which are, to some extent, considered to be mediated by Weyl fermions.

1.7 Structure of the thesis

Here is a concise detail of the organization of the thesis:

- Chapter 1: I have provided the general introduction of this thesis. Firstly, I summarized the role of topology in solid-state physics. It is followed by describing the phenomena anticipated and realized in Weyl semimetals. Among them, the theoretical background of two investigated topological excitations, chiral zero-sound in NbP and gravitational anomaly in NdAlSi, are discussed in detail.
- Chapter 2: I described the methodology work, including crystal growth methods, characterization of the sample through various techniques, a brief description of the cryogenic system used for transport measurement, and a self-made experimental setup for measurements of thermal conductivity. Finally, a description of mathematical equations for extracting various electrical and thermal parameters.

- Chapter 3: A summary of the article "Severe violation of the Wiedemann-Franz law in quantum oscillations of NbP (published in Physical Review B as a letter)" along with the article itself.
- Chapter 4: A summary of the article "Gravitational anomaly in the ferrimagnetic topological Weyl semimetal NdAlSi (published in Physical Review B as a letter)" along with the article itself.
- Chapter 5: Conclusion of the thesis.

Chapter 2

Methodology

This chapter describes the detailed methodology used in this thesis, including crystal growth methods, structural characterization, and transport measurements of the samples. Additionally, key components of the cryogenic system used for transport measurements are briefly introduced. In this thesis, the single crystals of the Weyl semimetal NbP and NdAlSi are selected for electrical and thermal transport measurements. These crystals were grown using chemical vapor transport (CVT) and flux growth techniques. The crystals are grown, preliminarily characterized using X-ray diffraction (XRD) for structural analysis and X-ray Laue diffraction to identify the crystallographic directions in the respective collaboration lab. In our home-assembled cryogenic system, electrical resistivity can be measured down to 1.8 K, and thermal conductivity can be measured down to 3.5 K in a magnetic field up to 14.5 T.

2.1 Single crystal growth

A single crystal is a periodic arrangement of atoms in three-dimensional space, making a continuous, uniform, and highly ordered structure. The synthesis of single crystals has attracted tremendous attention due to their wide range of applications, such as in the watch and jewelry industries, solid-state microelectronics, and laser technology. Specifically, single crystals play a crucial role in electronics, contributing to the manufacturing and performance of various electronic devices [134, 135]. For example, some of the key roles of single crystals are in solar cells, microprocessors, optoelectronic devices, and energy harvester modules [136]. In summary, the role of single crystals in electronic devices is crucial for fundamental as well as applied perspectives [137, 138].

On the fundamental scale, physical properties free from local disorder, long-range imperfection, and grain boundaries [139, 140] can be explored in a single crystalline phase of a material. However, some defects, especially point defects, are ubiquitously present in single crystals as they are in thermodynamic equilibrium due to the entropic disordering forces and thermal excitations at finite temperatures [141]. In the case of the poly-crystalline form of a sample, large-angle grain boundaries, and defects substantially affect the physical properties [142, 143]. Consequently, one can only measure an average value of the physical properties of all crystallographic directions rather than along a particular direction. In such a situation, a single crystal has an advantage over poly-crystalline form as it can measure anisotropy in various physical properties for their in-depth insights [144]. Furthermore, certain phenomena are only anticipated in the high-quality phase. For example, quantum oscillation is only realized under the clean limit of a material [72]. Therefore, it emphasizes the need for a high-purity single crystal for understanding their intriguing phenomena.

Crystal growth is a complex process that depends on conditions like temperature, pressure, solubility, solvent, supersaturation, etc. A slight disruption in one factor could influence the overall crystal growth. In this direction, enormous efforts are ongoing to grow crystals of high purity [141, 145]. Currently, several well-established crystal growth techniques are used depending upon the chemical and physical properties of a given material, their intended use, and the thermodynamic stability of participating constituents/components. For instance, CVT is preferred when a material has congruent melting, and the purity of the resultant single crystal is a matter of priority [141]. The flux method, used to grow single crystals from a molten state, is preferred for fast growth and large-sized crystals [145].

For a detailed characterization of a Weyl semimetal, precise control of crystallographic orientations is needed due to the requirement of aligning magnetic field and electric currents in certain crystallographic directions to observe interesting quantum effects such as chiral anomaly [12, 13, 14], anomalous hall effect [3, 4, 5, 6, 10] and chiral zero sound [119, 120, 121]. For example, the macroscopic manifestation of chiral anomaly, i.e., NLMR, is only expected in the colinear configuration of an electric and magnetic field along the separation of the Weyl points [12, 13, 14].

In this thesis, we selected two Weyl semimetals, NbP and NdAlSi, grown by CVT

[146] and flux methods [57], respectively. The following subsections will describe the general introduction of CVT and the flux method.

2.1.1 Chemical Vapour Transport

There are two types of the CVT technique: 1) stationary temperature profile (STP) and 2) time-varying temperature profile (TVTP) method. Usually, the former method has been widely practiced for growing single crystals [141]. In this thesis, the STP method was employed to grow the single crystal of NbP Weyl semimetal [146].

In the STP method, the participating component (or precursor), which is placed at one end of the ampoule with source temperature T_1, reacts with a gas (referred to as a transport agent, e.g., halogen-based such as I_2, Cl_2, Br_2), forming an exclusively volatile product. At the other end of the ampoule with growth temperature T_2, they undergo a reverse reaction, resulting in the crystallization of the precursor. Such component transportation from one end to the other end of the ampoule can result in a temperature difference, a change in free energy of the formation of substances, or changes in the relative pressures. During this growth process, temperatures T_1 and T_2 are kept constant with time; consequently, the supersaturation remains unaffected. The process depends on the length of the ampule used and parameters, namely, the concentration of the transporting agent, the temperatures T_1, T_2, and free energy change. Therefore, optimizing these parameters can improve the quality and size of growing crystals.

2.1.2 Flux growth method

The flux method has been practiced to grow single crystals for centuries. An enormous effort was made on this method during world war-II in search of a superior quality single crystal for military applications such as transducers in sonar and radar devices. Later, in 1948, the transistor's discovery drastically enhanced the demand for high-quality single crystals and, thus, the techniques used to grow them (see Chapter 15 in [141]). Currently, the method is used for large-scale industrial production of single crystals, nonlinear optical (NLO) crystals [147], the crystal of $\mathrm{YBa_2Cu_3O_{7-\delta}}$ (YBCO), where $\delta = 0 - 1$ [148], $\mathrm{BaTiO_3}$ [149] [141], yttrium iron garnet (YIG) [150], and many more [148].

In this method, the target material is mixed with a solvent (known as flux) and heated above the melting point of the solvent, $T_{melt}^{solvent}$, but below the material's melting point. The solvent helps in uniformly melting the material, and supersaturation is achieved at temperatures higher than $T_{melt}^{solvent}$. Therefore, the method used to grow a single crystal of those materials that melt incongruently at high temperatures [147]. The material dissolves into the solvent until it becomes supersaturated. After that, the mixture is slowly cooled down until it reaches the melting temperature of the solvent, crystallizing the material. Then, the solvent can be removed from the remaining mixture (solvent and crystals) through decanting, centrifugation, or dissolving in a suitable acid. However, sometimes, finding a suitable solvent and removing it can be challenging, leading to the formation of inclusions in the grown crystals. Single crystals of Weyl semimetal NdAlSi were grown using the flux method [57].

2.2 Structural characterization

X-rays are a form of electromagnetic radiation with wavelengths shorter than ultraviolet rays and longer than gamma rays. X-rays were discovered by Wilhelm Roentgen in 1895 and are named "X" rays because their exact nature was unknown at that moment. X-rays have been used to locate cracks in metal and human bones. Since X-rays have a wavelength in the range of 0.01 to 10 nm, comparable to the distance between periodically arranged atoms in a crystal, they are employed to determine the structural information of a crystal [151]. Moreover, these rays can penetrate deeply, providing information about a material's bulk structure.

A single crystal has a set of equally spaced parallel planes. Incident X-rays are diffracted by these planes [152, 153, 151, 91]; subsequently, these reflected X-rays undergo constructive interference, satisfying Bragg's Law, given by $2d\sin\theta = n\lambda$ [153], where d is the spacing between parallel planes, θ is the scattering angle, λ is the wavelength of incident X-rays, and n is a positive integer determining the order of the reflection. As d is constant in a crystal, Bragg's law is satisfied by varying scattering angles or shining polychromatic X-rays. The former way in which the angle varies is known as X-ray diffraction, while the latter way in which polychromatic X-ray is used is known as X-ray Laue diffraction.

In the X-ray diffraction method, intensity is plotted against 2θ, and the corresponding positions of the peaks provide the unit cell parameters. Additionally, the intensity of peaks is determined by the structure factor, which includes information on whether the plane can give the reflection or not [91]. Moreover, the structure factor embeds details of the arrangement of atoms in the crystal.

Here, X-ray and -Laue diffraction were used for the structural information and aligning the single crystals of selected Weyl semimetals, respectively. For the former analysis, the Rietveld refinement analysis is employed to fit the experimentally observed peak with those theoretically predicted using general structure analysis software [154, 155].

2.3 Cryogenic system

A cryogenic system is a specialized tool used in experimental condensed matter physics, materials science, and other scientific disciplines to perform low-temperature measurements. In transport measurements, the cryogenic system is equipped with a magnet. Therefore, the system can be used for temperature and field-dependent electro-thermal measurements. Here, the cryogenic systems are designed for performing experiments in a controlled environment, typically down to liquid helium temperatures and in the presence of an external magnetic field. These low-temperature experiments are crucial for studying the quantum dynamics of charge carriers and associated physical properties of materials. Fig. 2.1 presents a schematic of the cryogenic system used for electrical and thermal transport measurements. Some of the key parts of this system are listed below.

- Variable temperature insert (VTI): This component of the cryogenic system controls the variation of temperature, ranging from 1.8 to 300 K. The VTI is dipped into the helium reservoir (see Fig. 2.1), which is filled with liquid ^{4}He. A superconducting solenoid magnet is immersed into the helium reservoir around the VTI. Thus, the helium reservoir keeps the magnet and superconducting switch in their superconducting state. Temperatures of the ^{4}He can be lowered from 4.2 K (the boiling temperature of ^{4}He) by employing a rotary vacuum pump. The VTI has a needle valve (shown by a cyan arrow in Fig. 2.1) through which liquid helium is drawn from the helium reservoir. The construction of a needle valve is in a way that it causes a sudden pressure drop, leading to the cooling of ^{4}He by the "Joule-Thomson effect." Then, the cooled ^{4}He flows through the heat exchanger, which regulates the temperature of cold gas with the help of an integrated heater before entering the sample chamber. For sensing the temperature, the VTI has a thermometer placed on the heat exchanger or in the sample chamber (above the sample). In this way, the VTI controls and senses the temperature of the sample surroundings.

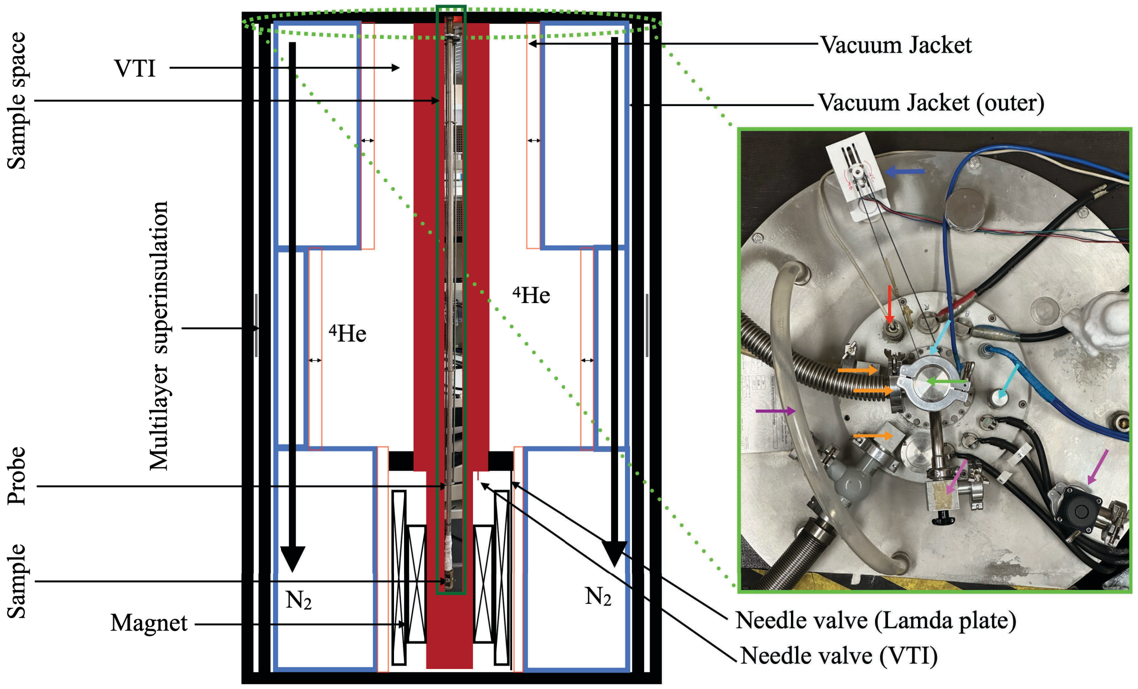

Figure 2.1: Schematic of the side view of cryostat (left image) depicting sample space, nitrogen, He reservoir, superconducting magnet, and VTI with sample probe. Top-view of the cryogenic system (right image) and various components are indicated by blue, red, cyan, light-cyan, magenta, dark-magenta, orange, and purple arrows pointing towards the stepper motor, connection to VTI heater, thermometer, needle valve (VTI), needle valve of lambda plate, vacuum ports for VTI and vacuum between nitrogen and He reservoirs, He-exhaust ports, nitrogen exhaust ports, respectively.

- The cryostat is equipped with a superconducting solenoid magnet operated with the Oxford power supply and can attain a magnetic field of 16 T (when cooled to temperature below the lambda point).
- We used Keithley's current (6221) and voltage voltmeter (2182A) for direct current (DC) and quasi-alternating current (AC) measurements, having a resolution in nano ampere and volt, respectively.
- Heaters are powered with LakeShore temperature controllers to supply the electric current, sense the voltage, and display the reading of the RhFe thermometer inside the VTI. The thermometer can be used in the temperature range of 1.4 to 325 K with good stability ± 10 mK (see LakeShore user manual).

- For He level indication, a superconducting wire was used to measure the helium level.
- The vacuum or pressure inside the sample chamber is regulated with the help of an electronic valve connected to a vacuum pump. To achieve the lowest possible temperature, a bypass valve is connected to the VTI He-exhaust.
- Lab view-interface software provides automation to all components of the cryostat.
- A stepper motor was used to set the position of the needle valve, thus, the helium flow.

2.4 Sample preparation for electrical and thermal transport

Samples with smooth and shiny surfaces were selected for electrical and thermal measurements. Later, the samples were cut into a rectangular shape using a wire saw (see Fig. 2.2). The cross-section area of the sample was kept small so that l/A (where A and l are the cross-section area and length of the sample) is significantly large. It is worth remembering that a sample with a reduced cross-section area minimizes the possibility of geometric effects that can affect the intrinsic properties (electrical and thermal conductivity).

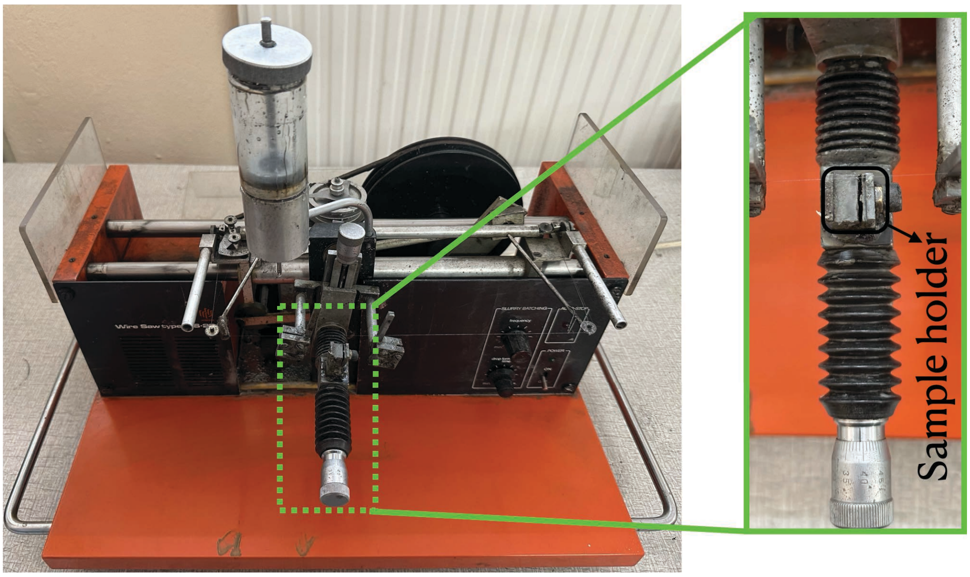

Figure 2.2: Wire saw used to cut a sample using a wire and a glycerin-suspended abrasive slurry that periodically drips on the intended cutting area. The slurry is filled in a vertical cylindrical tube. The wire moves back and forth on the sample with a frequency that can be adjusted according to the hardness of the sample. The target sample is mounted and fixed onto the sample holder (solid-black area). The position of the sample can be set through two screw gauges which are attached to the sample holder.

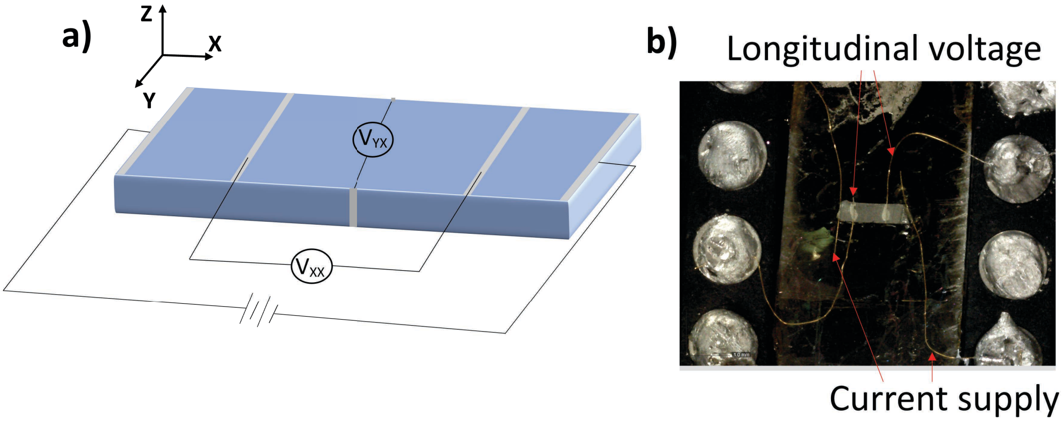

Figure 2.3: Crystals are cut into the rectangular bars using a wire saw. a) A schematic of the sample shown with two outer current contacts and two inner contacts over the surface for longitudinal voltage V_{XX} measurement. Two additional contacts were made across the thickness of the sample to measure Hall voltage V_{YX}. b) The measured sample with four contacts, two current and two contacts for measuring V_{XX}, is placed on 8-pin chip carriers glued with cryogenic tape. All contacts are made with gold wire and Ag-paste over the cross-section of the sample and then soldered to the pin of the chip carrier with indium.

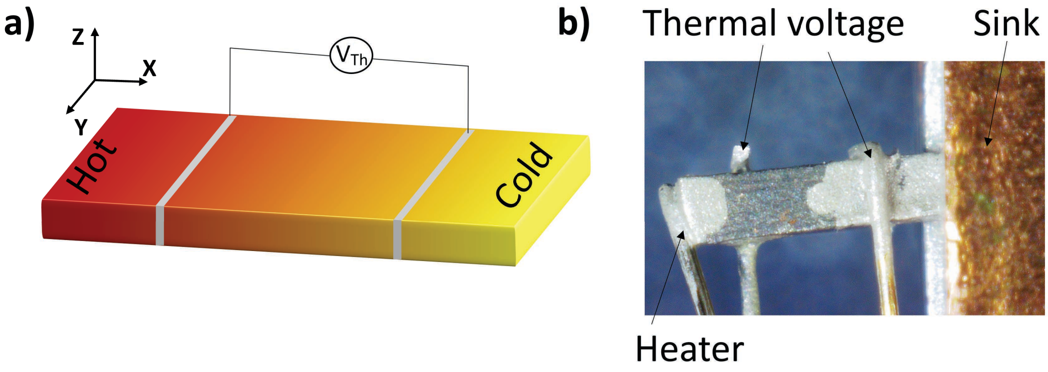

Figure 2.4: A rectangular sample is cut from the desired single crystal for thermal transport measurement. a) A schematic and b) the measured sample under applying temperature gradient ∇T. The thermal contacts are made over the cross-section of the sample with silver wire and silver paste, followed by connecting to a constantan-chromel thermocouple. Micro-measurements strain gauge as the heater was connected to the sample via a silver wire.

For instance, when dealing with high-mobility samples that have rough surfaces and large cross-sections relative to their length, magneto-resistance mechanisms that depend on geometry can make it difficult to interpret the experimental transport signature of the chiral anomaly, i.e., NLMR. Therefore, it is possible for extrinsic effects to overshadow or even pose a risk to the elucidation of the cause of NLMR, whether it is due to chiral anomaly in Weyl semimetal or not. However, thermal transport measurements are not influenced by extrinsic effects, particularly the current jetting effect, since the measurements are conducted in an open circuit.

2.5 Electrical transport measurement

Electrical transport typically refers to the physical phenomenon of how charge carriers, e.g., electrons and holes, move through the materials under the influence of external driving forces, such as an applied external electric field. It is crucial for understanding and exploring the behavior of charge carriers in different materials under certain conditions. In this thesis, electrical measurements have been carried out using a home-built probe (shown in Fig. 2.5), which can also be employed for angle-dependent measurements.

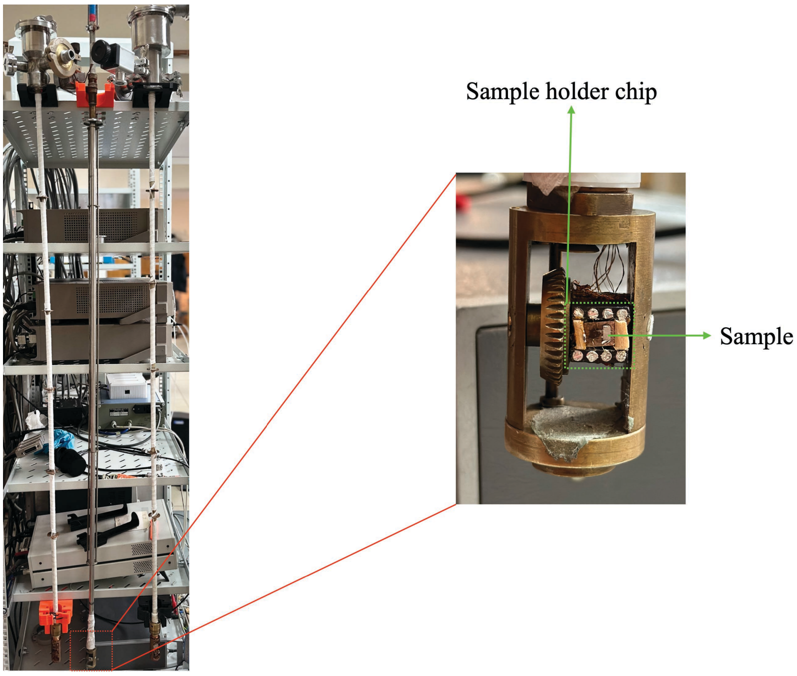

Figure 2.5: The transport measurement probes are shown; therein, the middle-one probe is used for electrical transport measurements. The setup for the measurement is shown in the zoomed-in view. The sample is mounted and soldered on 8-pin chip carriers, as shown by the green dotted area.

A Cernox chip thermometer, in addition to the RhFe resistive thermometer of VTI, was placed to measure the sample temperature accurately. The Cernox chip thermometer was bought with calibration data, and its reading is expected to be nearly independent of B. Six contacts were constructed using 50 μm thick gold wire with Ag-paste. Contacts were made across the cross-section of the sample to maintain the homogeneous current flow. Such construction of contacts can also minimize the risk of the current jetting effect.

The measurements were performed in the temperature and magnetic field range from 1.8-300 K and -14.5 to 14.5 T, respectively. The measured resistance R was converted into resistivity ρ using Ohm's law $\rho = R \cdot \frac{l}{A}$. The field sweeps (up and down) are used to extract the symmetric and anti-symmetric components of $\rho(B)$. In electrical transport, the possibility of contact misalignment can be corrected by applying the symmetrization/anti-symmetrization process on $\rho_{xx}(B)/\rho_{xy}(B)$. The symmetric and anti-symmetric components of resistivity are calculated at a finite temperature T as follows:

$$\rho_{xx}(B,T) = \frac{1}{2}[\rho_{xx}(+B,T) + \rho_{xx}(-B,T)], \tag{2.1}$$

$$\rho_{xy}(B,T) = \frac{1}{2}[\rho_{xy}(+B,T) - \rho_{xy}(-B,T)], \tag{2.2}$$

where ρ_{xx} is longitudinal resistivity and ρ_{xy} : is transverse or Hall resistivity.

During measurements, we observed a lagging (leading) of the magnetic field 0.05 T to the actual field, which was corrected by adding (subtracting) 0.05 T magnetic field value in the up (down) sweep of the magnetic field.

The study of electrical properties can reveal various parameters, allowing us to understand the underlying physics. For example, by performing a comprehensive analysis of quantum oscillation, one can gain valuable insight into Fermi surface morphology, providing the effective mass of charge carriers, Fermi energy, etc [72]. From Hall resistivity, one can calculate the mobility of electrons or holes. Using the Drude model, one can calculate the average transport scattering time, a crucial parameter in many conducting materials. Additionally, we fitted the longitudinal resistivity with the chiral anomaly Eq. 1.7 to determine inter-valley scattering time. In the upcoming subsections, we have discussed these analyses in detail.

2.5.1 Quantum oscillation analysis

Quantum oscillations are defined as a periodic behavior observed in certain physical properties (in our case, electrical/thermal conductivity) of materials under applying the magnetic field at low temperatures. The oscillation observed in electrical resistivity is called SdH [156] [157], and the theoretical aspect of it is described in chapter 1.

We observed quantum oscillations in both selected Weyl semimetals (NbP, NdAlSi) within the high magnetic field range [121, 106]. The oscillatory component of $\rho(B)$ was extracted by fitting the resistivity with a suitable polynomial function in a magnetic field window from B_{min} to B_{max}, which was then subtracted from the resistivity. It is a standard method to remove the non-oscillatory component. The resulting oscillatory component was plotted against $1/B$ to visualize the period and amplitude of the oscillations. Usually, a fast Fourier transformation is performed to identify the present frequencies of the oscillation.

Alternatively, one can estimate the frequency from a distance between two successive minima/maxima of the oscillatory components in case of a few frequencies. Too many existing frequencies make the later approach quite challenging for determining the frequency precisely. The temperature-dependent amplitudes of oscillation were fitted with temperature damping factor $R_T = \frac{\alpha n T}{\sinh(\alpha n T)}$ (the first term in L-K formula [156]) for extracting the effective mass,

$$m^* = \alpha \frac{e\hbar B_{effective}}{2\pi^2 k_B}, \tag{2.3}$$

where $B_{effective} = (B_{min} + B_{max})/2$, $\alpha = \frac{2\pi^2 k_B m^*}{e\hbar B_{effective}}$ is a fitting parameter and n is the harmonic number.

We utilized k_F and Fermi velocity ($\nu_F = \frac{\hbar k_F}{m^*}$) for estimating Fermi energy (ϵ_F):

$$\epsilon_F = \hbar \nu_F k_F. \tag{2.4}$$

2.5.2 Extraction of mobility

Hall resistivity (ρ_{yx}) measurements have been used to characterize a conducting material since the discovery of the Hall effect by Edwin Hall in 1879. It provides information on the sign/type of charge carrier (electrons or holes), carrier concentration, and mobility of charge carriers. The measurements are widely used in research as well as industry for extracting carrier concentration and mobility of charge carriers. Experimentally, the Hall resistivity calculated as:

$$\rho_{yx} = R_{yx} \cdot t, \tag{2.5}$$

where $R_{yx} = \frac{V_{YX}}{I}$; I is an electric current, V_{YX} measured Hall voltage, and t is the thickness of the sample.

We performed the Hall resistivity down to 1.5 K and in the magnetic field up to 14.5 T. The Hall resistivity is calculated using the Eq. 2.5. For determining the carrier density, we fitted $\rho_{yx}(B)$ at a constant temperature with a single band model (linear function in B) in the high magnetic field range for NbP.

$$\rho_{yx}(B) = R_H \frac{I \cdot B}{t}, \tag{2.6}$$

where $R_H = \frac{1}{ne}$ is Hall coefficient and n is the density/concentration of charge carriers.

In the high magnetic field regime, when $\rho_{yx}(B)$ shows linear with the magnetic field, it can be assumed that either electrons or holes dominate the charge transport depending upon the sign of the slope of $\rho_{yx}(B)$. For example, the positive slope value of $\rho_{yx}(B)$, R_H, for positive/negative magnetic field sweeps indicates the electron/holes dominating the samples' charge carriers.

The mobility of charge carriers in a material can be determined from the Hall coefficient (R_H) and ρ_{xx} using a single band model:

$$u(T) = \frac{R_H(T)}{\rho_{xx}(T)}, \tag{2.7}$$

where u is the mobility of the charge carriers at a finite temperature.

2.5.3 Inter-valley and transport relaxation time

Inter-valley scattering τ_{WP} was determined by fitting the longitudinal magneto-conductivity $\sigma_{xx}(B)$ with the semi-classical chiral anomaly equation (cf. Eq. 1.7). While calculating τ_{WP}, effective mass m^*, Fermi velocity, and Fermi energy were used. The Fermi energy was estimated from the Fermi wavevector (see Eq. 2.4), which was determined using Onsager relation (Eq. 1.4). Transport time $\tau_{trans} = \frac{um^*}{e}$ was estimated and was compared with τ_{WP}. For chiral limit, τ_{WP} should be longer than τ_{trans}. In the case of gravitation anomaly phenomena, the former can also be estimated by fitting the longitudinal magneto-thermal conductivity $\kappa_{xx}(B)$ with a gravitational contribution (cf. Eq. 1.19) to thermal conductivity in the high magnetic field range. In both transport measurements (electrical and thermal), τ_{WP} is the time scale that dictates the dynamics of Weyl fermions.

2.6 Thermal transport rig

Our thermal transport probe consists of two constantan-chromel type-E thermocouples, a sample holder (made of copper), a thermal shield, resistive chip heaters, a BeO connector/very thin laminate chip, Kevlar wool (low thermal conductivity), Phosphor-Bronze coils, and five gears which provide us rotational freedom.

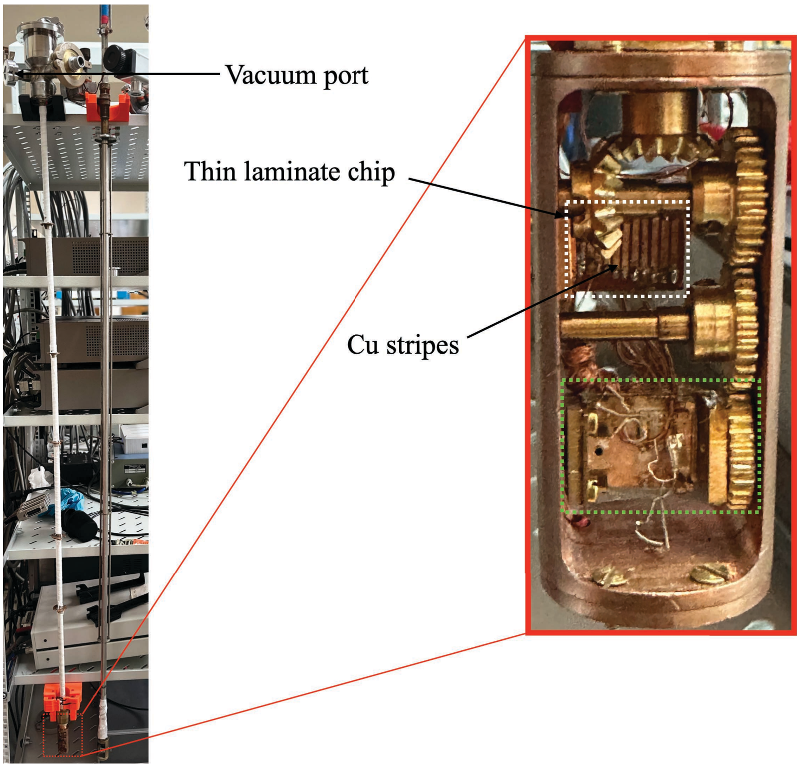

Figure 2.6: A homemade thermal transport probe (leftward). The end of the probe is seen in the zoomed-in view (rightward). A dotted green area represents the thermal heat transport setup. The whole setup was vacuum-sealed during the measurement by covering it with a brass vacuum can. This also prohibits the unintentional flow of ^{4}He during the measurements. In this setup, the hanging wire of thermocouples and heaters is suspended on the thermally insulating Kevlar threads.

The preparation of the major components of the probe is to be discussed in the coming subsections.

2.6.1 Spot welding machine

The capacitance-discharging spot welding machine was used to join the thermocouple wires in the form of point contact. The machine was made using a 470 μF, a rectangular copper plate, and a copper needle. The welding mechanism of this machine involves charging a capacitor with a voltage supply and then suddenly discharging it. While discharging (touching the needle on the copper plate), it generates sufficient heat to melt the wire and make thin contacts.

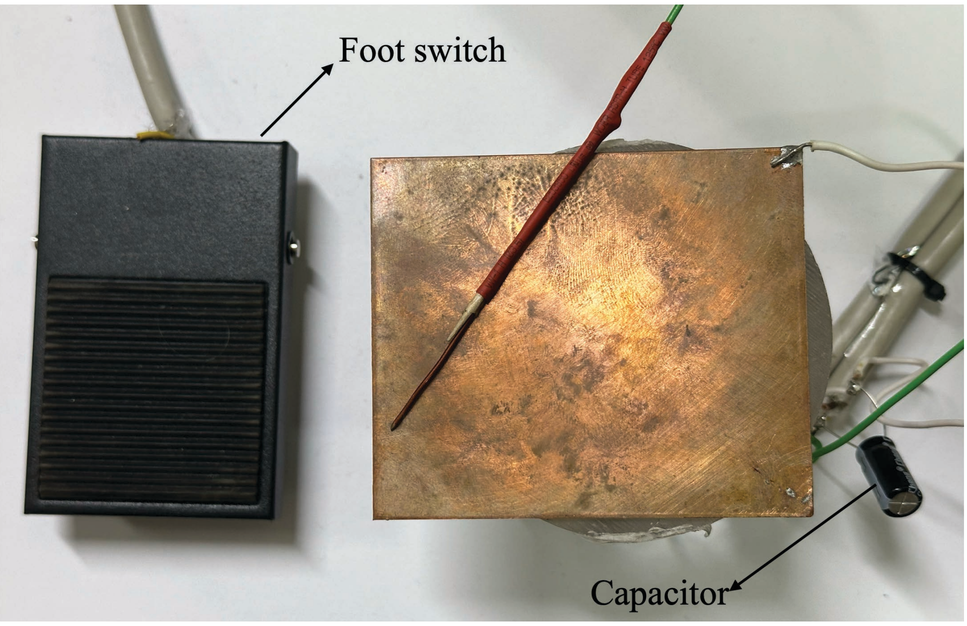

Figure 2.7: The figure shows a capacitor discharge spot welding. One leg of the capacitor is connected to a copper plate, and another is connected to a copper needle through a foot switch. The switch shorts or discharges the capacitor, providing easy handling while welding.

2.6.2 Preparation of thermo-couples

Type-E thermocouples were made using three coils (two coils of constantan and one coil of chromel) of two dissimilar materials, chrome (nickel with 10% chromium) and constantan (nickel with 45% copper), as shown in Fig. 2.8.

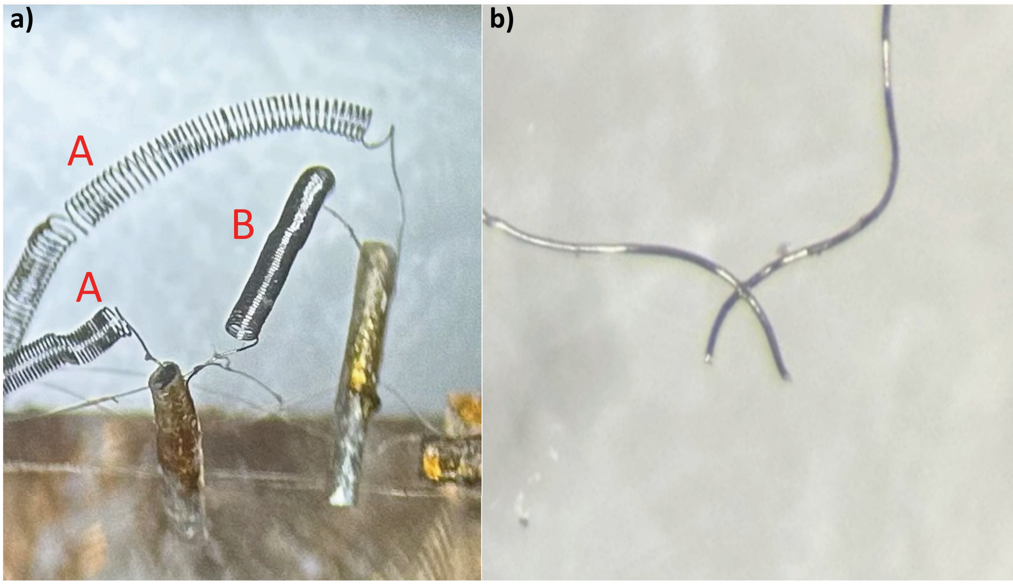

Figure 2.8: a) Type-E constantan-chromel thermocouple wherein two coils of chromel (A) and one coil of constantan (B) are attached to the silver wires to provide better support to the junctions. b) The junction after welding the legs of the coils without burning the wires.

The legs of the thermocouple are joined using a capacitance discharging spot welding, forming a junction. Then, the junctions are covered with two components, epoxy paste, for electrical insulation and mechanical durability. Lastly, the insulated junction is thermally contacted with thick silver wires. Other free legs are connected to the BeO chip and used to measure the resulting thermal voltage generated in the presence of the temperature gradient.

The following equations can be written using the Seebeck effect for calculating the temperature difference between two junction points:

$$V = S \cdot \Delta T \tag{2.8}$$

$$\begin{aligned}
V_1 &= S_B(T_1 - T_0), V_2 = S_A(T_2 - T_1), V_3 = S_B(T_0 - T_2), \\
V_{\text{total}} &= V_1 + V_2 + V_3 \\
&= S_B(T_1 - T_0) + S_A(T_2 - T_1) + S_B(T_0 - T_2) \\
V_{\text{total}} &= S_B - S_A(T_1 - T_2), \qquad (2.9)
\end{aligned}$$

where S_A, S_B, and T_1, T_2 are Seebeck coefficient of chromel and constantan, and the temperature at junction 1 and 2, respectively.

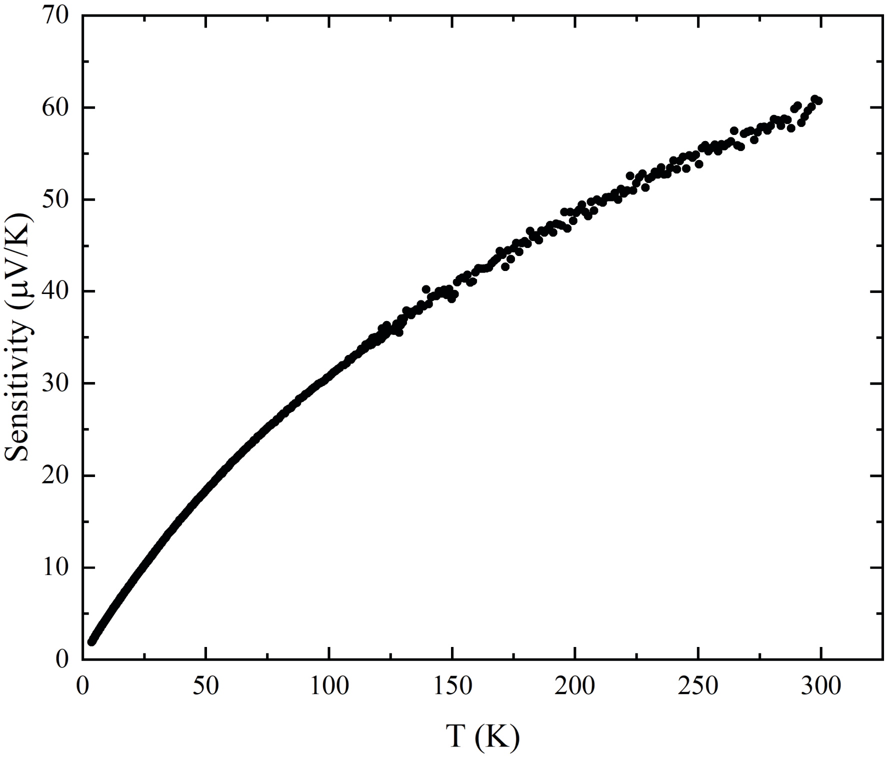

Figure 2.9: Sensitivity of type-E constantan-chromel thermocouples with temperature. The sensitivity is multiplied by the measured thermal voltage to convert it into the corresponding temperature gradient.

2.7 Thermal transport measurement

A sample's response is measured under an external temperature gradient in thermal transport measurements. How one applies the gradient defines the type of method employed. In this thesis, we used the steady-state method. The method refers to the condition where heat flow leads to thermal equilibrium over a finite period. In other words, the temperature distribution within the system does not change with time. In our case, we used two constantan-chromel thermocouples and one heater to measure thermal conductivity.

A thermal transport setup is shown in Fig. 2.10, where one end of the sample is attached to the base (copper block, heat sink), and the opposite end is connected to the heater through a 100 μm-thick silver wire using Ag-paste or two-component conductive epoxy. One thermocouple was attached across the sample to measure the temperature difference, and a second thermocouple was placed between the heater and the base. The latter thermocouple provides the temperature difference ΔT_{HB} between the heater and sample base.

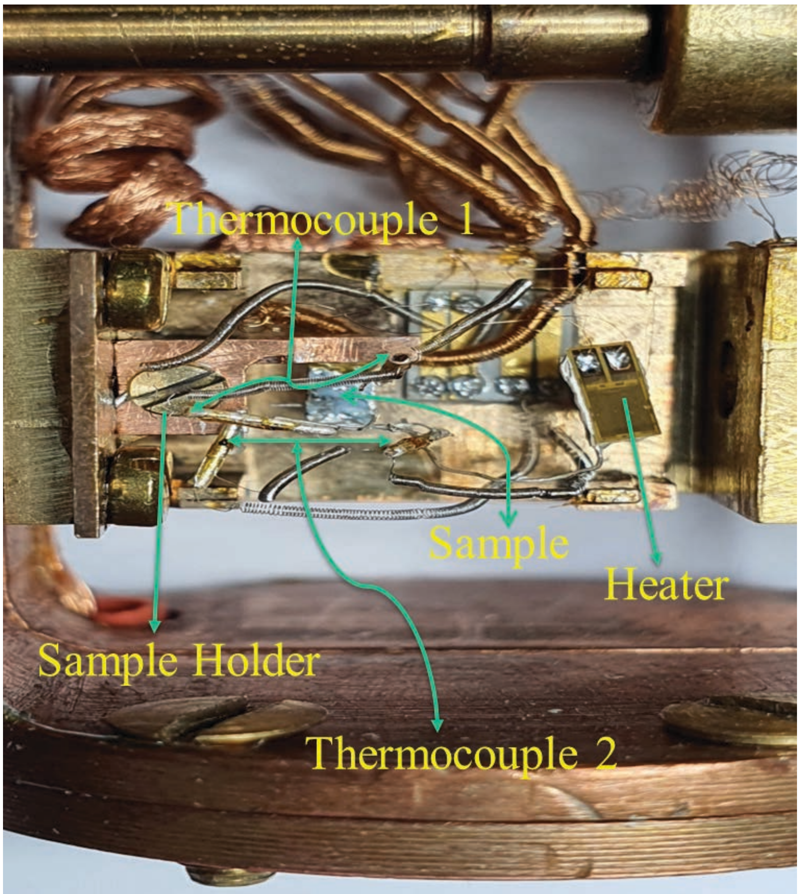

Figure 2.10: Thermal setup including sample, which was used to measure the thermal conductivity. The sample holder was screwed with a heat sink. The heater and hanging coils of thermocouples are suspended on insulating Kevlar threads. Thermocouple 1 is connected across the sample, and thermocouple 2 is connected between the heater and heat. The entire setup is encapsulated with an Ag-thermal shield and then with a brass-can for vacuuming the setup and restricting the ^{4}He flow during the measurements.

A Cernox resistive thermometer is placed at the base, giving the value of temperature T_B. Using T_B and ΔT_{HB}, we can calculate the average temperature of the sample T_{mean} while performing the measurements.

$$T_{mean} = T_B + \frac{\Delta T_{HB}}{2}.$$

In the steady-state method, a heater is on for a finite time (1- 5 minutes), allowing the sample to attain thermal equilibrium at temperature $T_{heater-on}$. Subsequently, the heater is turned off to facilitate cooling, accomplishing a steady or thermal equilibrium state at temperature $T_{heater-off}$. Thus, a steady temperature gradient was established across the sample. In our case, the cycle is repeated over the temperature range of 3.5 to 300 K. Approximately the last 25% (or after established thermal equilibrium) data of the heater on and off state (see in Fig. 2.11) were considered for the analysis. Lastly, the heater-off reading was subtracted from the heater-on reading, and the resultant corresponds to the temperature difference $\Delta T = T_{heater-on} - T_{heater-off}$ at the mean temperatures of the sample. The thermal conductivity is calculated using the formula:

$$\kappa = \frac{l}{A}\frac{P}{\Delta T}. \tag{2.10}$$

Where P,l, A, and ∇T are the power (I^2R; I is electric current and R is the resistance of chip heater) supplied to the heater, the distance between two longitudinal thermal contacts (see Fig. 2.11), the cross-section of the sample, and the steady state temperature difference, respectively.

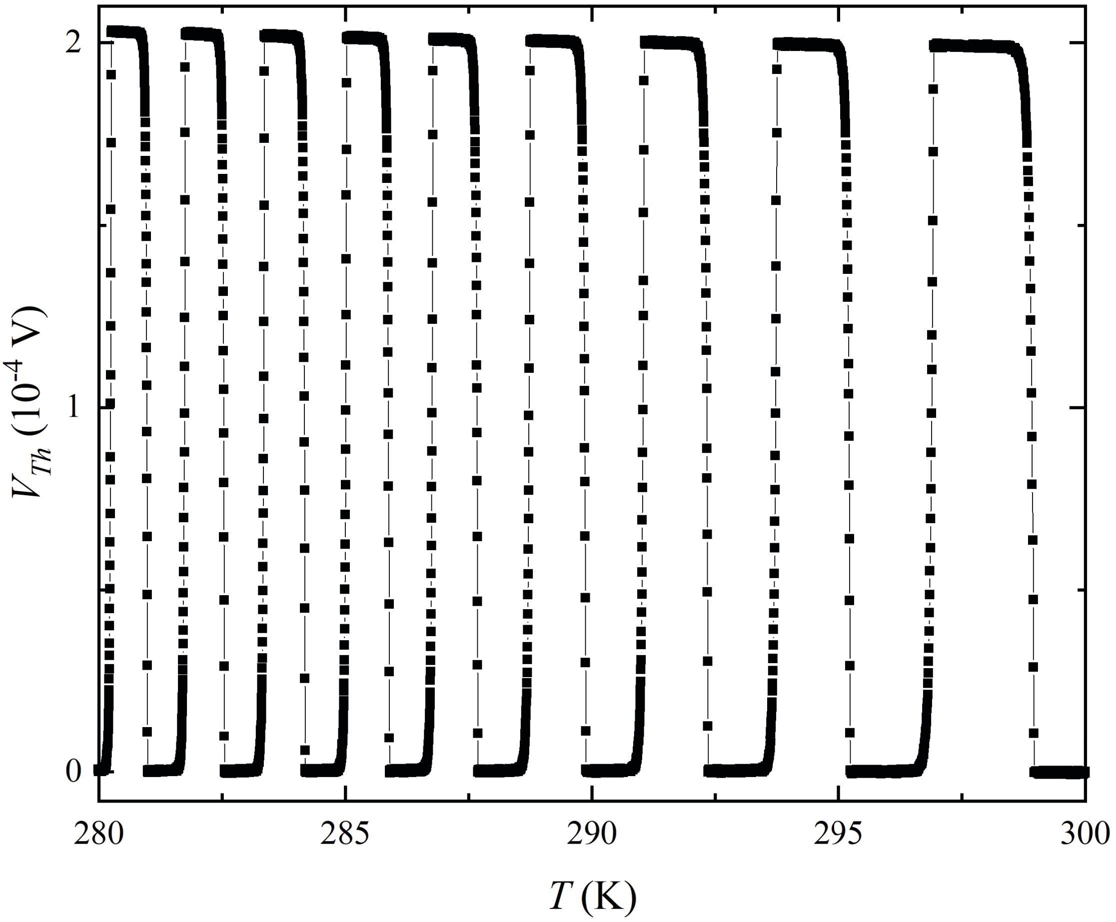

Figure 2.11: It shows the measured thermal voltage V_{Th} in the temperature range 280-300 K. During the measurements, the heater is periodically powered on. As a result, the thermal voltage is saturated to maximum and minimum values while the heater is on and off in finite time intervals, respectively.

2.7.1 Minimization of heat losses

It is important to note that the accuracy of the steady-state method used to calculate the thermal conductivity of a sample relies on the assumption that all the heat generated by the heater passes through the sample. In order to determine the thermal conductivity (κ), one needs to know the exact power (P) used. However, the accuracy of thermal measurements can be compromised by heat losses. These losses occur when heat from the heater finds alternative paths to escape rather than passing through the sample. Modes of heat loss encompass radiation, conduction, and diffusion. In addition, a temperature drop at the junctions or through the connecting wires can also be a source of uncertainty in the actual temperature of the sample. This was resolved by using two different connected thermocouples. Therefore, minimizing heat loss is crucial in heat transport measurements to reduce the uncertainty in measured thermal conductivity. To mitigate heat losses by potential modes, we employ the following strategies:

- Heat loss through conduction: Long and thin (25 μm) phosphor bronze coils (low thermal conductivity) coated with an insulating layer are used. The ends of the coils are connected to a gold (copper) strip made on the Beryllium oxide chip/very thin laminate, acting as a heat sink. In this way, the end of the connecting wire can be placed at the same temperature. Such construction prevents heat transfer from the probe wires, which are at room temperature at the top connector. Equalizing the temperature of the connectors will also reduce additional thermoelectric signals. The thermocouples are also made with long thin wires (25 μm), and their leads are connected to a Beryllium oxide chip, thus eliminating any unintentional additional temperature difference caused by the surroundings.

- Radiation heat losses: The silver radiation shield covers the green dotted area (where the sample, sample heater, and thermocouples are placed); see Fig. 2.6. An additional sample heater was placed on the surface of the radiation shield. The heater is mounted in the way to face the sample heater, and the same current was applied to both heaters to achieve a thermal equilibrium or minimize a temperature difference between them.

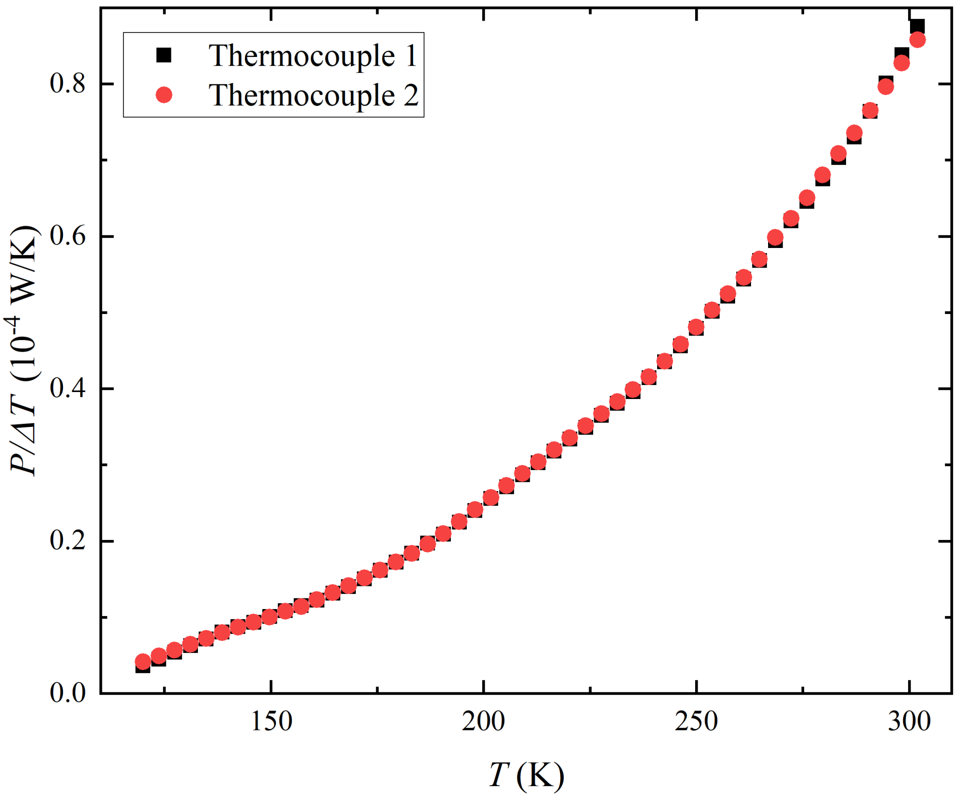

Figure 2.12: Radiation losses by the heater itself. Both thermocouples (1 and 2) were connected between heat and base without a sample. The figure represents the applied power normalized with measured ΔT solid-red circle and black square) by thermocouples 1 and 2 with temperature, respectively. The data confirms that both thermocouples measure the same ΔT.

We estimate the radiation losses by the heater itself (see Fig. 2.12) and consider them while analyzing the data. The ratio of applied power and ΔT data (solid-red circle in, Fig. 2.12) was fitted with an analytical function pT^t, giving fitting parameters $p \approx 1.79e^{-12}$ and $t \approx 3.11$. We realized that radiation losses calculated by the function pT^t at low temperatures are significantly small.

- Diffusion: During the measurement, the sample probe is connected to a vacuum turbo pump to minimize the possibility of heat diffusion by gas (for example, He). Successful minimization of heat loss is indicated by no significant disturbance being observed in the vacuum state during the measurement process.

2.7.2 Magneto-thermal conductivity

The thermal conductivity measurements were carried out in the magnetic field (up to 14.5 T) at a constant temperature. During these isothermal field sweeps, the heater is kept on during the entire sweep (-14.5 to 14.5 T). In a magnetic material, the heater-off readings are sensitive to the magnetic field. In our case, the heater-off reading was taken from temperature-dependent thermal conductivity at a constant magnetic field. The temperature gradient in the off state of the heater is given:

$$\Delta T_{off}(T,B) = \frac{l}{A}\frac{P}{\kappa(T,B)}, \tag{2.11}$$

where $\kappa(T,B)$ is thermal conductivity at constant magnetic field.

In our case, we carried out a temperature ramp from 4 to 300 K at constant magnetic field B = 1, 5, 10, 14.5 T. After that, one can extract the iso-thermal temperature gradient of the sample in the magnetic field range of 0-14.5 T. The net temperature gradient of the sample in the magnetic field at constant temperatures:

$$\Delta T_{net}(H,T) = \Delta T_{on}(H,T) - \Delta T_{off}(T,H). \tag{2.12}$$

Similar to electrical conductivity/resistivity, the symmetric component of longitudinal thermal conductivity can be given:

$$\kappa_{xx}(B,T) = \frac{1}{2}[\kappa_{xx}(+B,T) + \kappa_{xx}(-B,T)]. \tag{2.13}$$

Noteworthy, one should always calculate the thermal resistivity rather than thermal conductivity and then invert it to get thermal conductivity. In our case, there is no thermal Hall in the parallel configuration of ∇T and magnetic field B ($\nabla T \parallel B$). Therefore, we directly calculated thermal conductivity using Eq. 2.10.

2.7.3 Chiral zero-sound model

The analysis of $\kappa(B)$ is useful in determining the parameters such as velocity of sound mode, relaxation time, Debye temperature, etc. In the case of NbP, we observed huge quantum oscillation, which was ascribed to CZS (an additional heat channel, summarized in chapter 3). The measured total magneto-thermal conductivity is fitted with the theoretical contribution of CZS using Eq. 1.18. The following steps elucidate the fitting procedure for $\kappa(B)$ with CZS thermal conductivity:

- CZS contribution to total thermal conductivity is calculated using the Eq. 1.18; therein, k_F, Λ is calculated using dominate frequency, and ν_F was theoretically estimated.
- An expression $\kappa_{CZS}(B)+$c (where c is a constant) was fitted with total thermal conductivity in the magnetic field range 0-14.5 T. Noteworthy, all theoretical expressions must be converted into SI units before fitting the equation.

From this fitting, we can get the CZS relaxation time, velocity, and Debye temperature. Eventually, the chiral limit of the Weyl semimetal is evaluated. The following equations expressed these parameters:

Velocity of chiral zero sound:

$$C(B) = \frac{eB}{4\pi^2\beta(B)}\sqrt{\zeta_0^2 - \zeta_1^2}, \tag{2.14}$$

where, $\beta(B) = \frac{\mu^2}{2\pi^2\nu_F^3}$, factor $\sqrt{\zeta_0^2 - \zeta_1^2}$ was theoretically calculated.

Debye temperature:

$$\Theta_{CZS} = \frac{\hbar\Lambda C(B)}{k_B}. \tag{2.15}$$

Relaxation time τ_{CZS}:

$$\bar{\kappa} = \frac{\kappa_{CZS}(B)}{\tau_{CZS}k_B\Lambda^3\nu_F^2 N_{CZS}}, \tag{2.16}$$

where $\bar{\kappa}$ is a dimensionless quantity and determined experimentally.

Chiral limit:

$$\frac{\tau_0}{\tau_{CZS}} \ll 1, \tag{2.17}$$

where τ_0 is transport relaxation time and was calculated from the experimental value of electric conductivity using the Drude model for Weyl semimetal. The Fermi wavevector is calculated using the Onsager relation Eq. 1.4, the chemical potential was calculated using the Fermi vector of dominating frequency, and Fermi velocity was theoretically estimated.

2.8 Measurement errors in absolute values

In transport measurements, the absolute error in a measured quantity is associated with the instruments' resolution, such as voltmeters and current sources. Quantifying errors in our self-built setup is challenging; however, we can qualitatively determine their impact on our measurements.

- In transport measurements, we measure voltage, which may have some uncertainty while measuring it. This uncertainty propagates to the derived quantities, such as electrical resistivity and thermal gradient, thus in thermal conductivity. In our case, the voltmeter and current source have a resolution of nano-volts/ampere. At the same time, the amplitude of the measured signal is at least two orders larger than the meter's resolution, indicating a substantial signal-to-noise ratio. In thermal transport measurements, to enhance the thermal voltage signal, we use an EM Electronics A20a DC nanovolt amplifier. This provides a quite good signal-to-noise ratio in voltage measurements, down to 1.8 K and 4 K in electrical and thermal transport measurements. Therefore, we believe the uncertainty associated with thermal voltage or gradient is unlikely to be a substantial source of error in our measurements.
- Geometric factor of the sample - l/A can serve as a significant source of systematic error, especially in thermal conductivity measurements. In our case, we expect it to have uncertainty of up to 10%.
- Heater power: There is uncertainty in the power generated by a resistive heater I^2R. In this case, the current source employed to excite the heater exhibits a resolution at the nanoampere level. A potential problem could be the change in resistivity of the heater with temperature or magnetic field. This has been verified as negligible. Hence, the uncertainty associated with heater power is smaller than the uncertainty related to the geometrical factor of the sample.

Chapter 3

Chiral-zero sound

3.1 Summary: Severe violation of the Wiedemann-Franz law in quantum oscillations of NbP

Here, we performed the transport measurements on Weyl semimetal NbP, which hosts multiple pairs of Weyl points. Firstly, a single crystal of NbP was characterized by electrical measurements down to 1.7 K and in a magnetic field up to 14.5 T. We observed quantum oscillation with several frequencies: 4.9 (F1), 9.1 (F2), 16 (F3), 29 (F4), and 40 (F5) T when magnetic field and electric current were applied parallel to each other along the c-axis.

Likewise, two nearly the same frequencies appear in the thermal conductivity to their counterparts from SdH, F3 = 15 T and F4 = 30 T when $\nabla T||B||c$. Remarkably, the frequencies that occur in thermal conductivity are in antiphase. Moreover, they have two orders of magnitude larger than those observed in the electrical thermal conductivity, calculated from electrical conductivity using the Wiedemann-Franz law.

In the case of non-compensated Weyl semimetals, such large thermal conductivity is unlikely related to ambipolar contribution at temperatures far below the Fermi temperature. The lattice thermal conductivity was estimated by fitting the $\kappa(T)$ with $aT + bT^3$ function (where aT and bT^3 are electronics and lattice contributions to thermal conductivity, respectively). This was done under the assumption that the mean free path of electron and phonon is temperature-independent at low temperatures. Given the fact that lattice thermal conductivity shows weak magnetic field dependence, we believe that phonons contribution appears not to be a good candidate to explain the behavior of $\kappa(B)$. Alternatively, we estimated the chiral zero sound contribution to the thermal conductivity using the theoretical model given by *Z. Song and X. Dai*. This contribution turns out to fit the experimental thermal conductivity quite well. Thus, chiral zero sound serves as an additional chargeless heat channel, drastically violating the Wiedemann-Franz law.

3.2 Authors statement and publication 1

Name and surname: Pardeep Kumar
MagToP (ON6.6, Weyl group)
Institute of Physics, Polish academy of sciences,
Aleja Lotnikow 32/46, Warsaw, 02-668, Poland

STATEMENT

I declare that I am a co-author of the publication:

P. K. Tanwar, M. S. Alam, M. Ahmad, D. Kaczorowski, and M. Matusiak, Severe violation of the Wiedemann- Franz law in quantum oscillations of NbP, Phys. Rev. B 106, L041106 (2022).

I contributed to the following:

- Prepared the thermal transport setup under the mentorship of Dr. hab. Marcin Matusiak
- Conducted experimental measurements, including electrical and thermal conductivity measurements, at temperatures as low as helium temperature and magnetic fields up to 14.5 T
- Developed Python software for analyzing the results obtained from electrical and thermal measurements
- Contributed in interpreting the experimental results
- Participate in conceptualizing the idea of chiral zero sound
- Worked on writing the original manuscript and reviewed and edited it.
- Participated in addressing all the criticisms raised by the reviewers during the review process

Place: Warsaw
Date and Signature:
20/04/2024

Name and surname: Md Shahin Alam
MagToP (ON6.6, Weyl group)
Institute of Physics, Polish academy of sciences,
Aleja Lotnikow 32/46, Warsaw, 02-668, Poland

STATEMENT

I declare that I am a co-author of the publication:

P. K. Tanwar, M. S. Alam, M. Ahmad, D. Kaczorowski, and M. Matusiak, Severe violation of the Wiedemann- franz law in quantum oscillations of NbP, Phys. Rev. B 106, L041106 (2022).

I contributed to the following:

- ✓ Discussion of the experimental results
- ✓ Writing section- Review & Editing

Place: Islampur, India

Date and Signature: 13/04/2024

Md. Shahin Alam.

Name and surname: Mujeeb Ahmad
MagToP (ON6.6, Weyl group)
Institute of Physics, Polish academy of sciences,
Aleja Lotnikow 32/46, Warsaw, 02-668, Poland

STATEMENT

I declare that I am a co-author of the publication:

P. K. Tanwar, M. S. Alam, M. Ahmad, D. Kaczorowski, and M. Matusiak, Severe violation of the Wiedemann- franz law in quantum oscillations of NbP, Phys. Rev. B 106, L041106 (2022).

I contributed to the following: I had performed the Hall measurements in this study.

Place: Warsaw

Date and Signature: Mujeeb Ahmad
27/01/2024

Name and surname: Prof. Dariusz Kaczorowsk
Institute of Low Temperature and Structure Research,
Polish Academy of Sciences, ul. Okólna 2, 50-422 Wrocław, Poland

STATEMENT

I declare that I am a co-author of the publication:

P. K. Tanwar, M. S. Alam, M. Ahmad, D. Kaczorowski, and M. Matusiak, Severe violation of the Wiedemann- Franz law in quantum oscillations of NbP, Phys. Rev. B 106, L041106 (2022).

I contributed to the following:

- Provided crystals of NbP
- Review and editing of the manuscript

Place: Wrocław
Date and Signature: 5.02 24 D. Kaczorowski

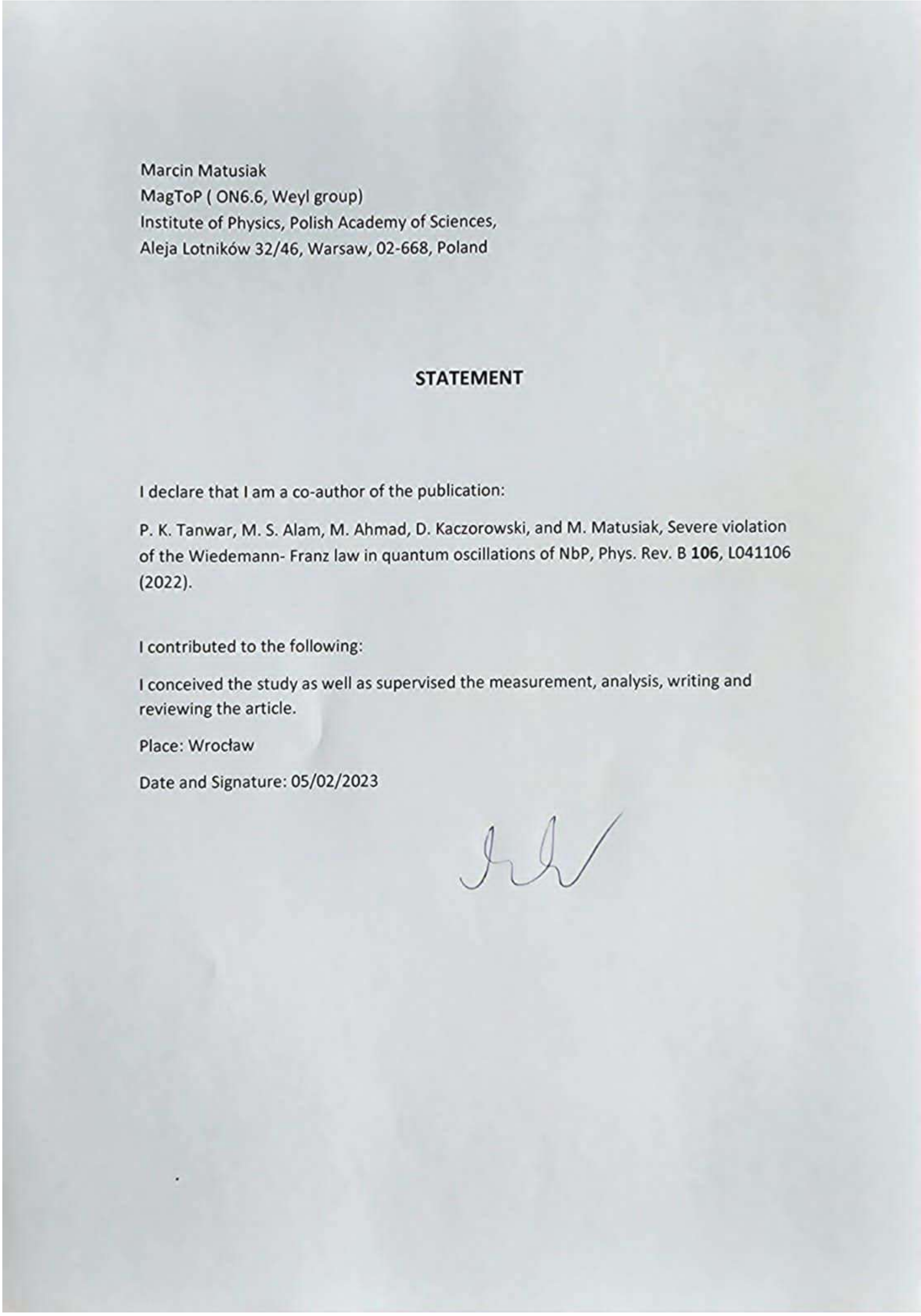

Marcin Matusiak
MagToP (ON6.6, Weyl group)
Institute of Physics, Polish Academy of Sciences,
Aleja Lotników 32/46, Warsaw, 02-668, Poland

STATEMENT

I declare that I am a co-author of the publication:

P. K. Tanwar, M. S. Alam, M. Ahmad, D. Kaczorowski, and M. Matusiak, Severe violation of the Wiedemann- Franz law in quantum oscillations of NbP, Phys. Rev. B **106**, L041106 (2022).

I contributed to the following:

I conceived the study as well as supervised the measurement, analysis, writing and reviewing the article.

Place: Wrocław

Date and Signature: 05/02/2023

Chapter 4

Gravitational anomaly

4.1 Summary: Gravitational anomaly in the ferrimagnetic topological Weyl semimetal NdAlSi

In this article, we have demonstrated the existence of the gravitational anomaly in a semi-classical regime of NdAlSi. The discovered effect is a unique thermal property of Weyl semimetals when ∇T is applied parallel to the magnetic field and along the separation of Weyl nodes. Gravitational anomaly leads to an imbalance in temperature between Weyl nodes of opposite chirality while the number of Weyl fermions remains the same in respective nodes. Weyl semimetals provide a promising platform for testing the relativistic field theories of chiral fermions through table-top transport experiments. The macroscopic manifestation of the quantum anomaly can be observed in the transport coefficients of these materials due to the formal link between the gravitational field and ∇T.

We observed an increase in thermal conductivity with a magnetic field resulting from the gravitational anomaly. Remarkably, this increase of $\kappa(B)$ is related to the chiral magnetic effect contribution to electrical conductivity in a way predicted by the classical Wiedemann-Franz law. What distinguishes this discovery is its resilience against external artefacts, unlike the chiral magnetic effect.

Here, lattice thermal conductivity was estimated by scaling the phononic contribution to the specific heat of LaAlSi in the temperature range 15-23 K with the remaining non-electronic thermal conductivity of NdAlSi, after subtracting the electronic thermal conductivity. For estimating the phononic contribution, the specific heat of LaAlSi was fitted with $aT + bT^3$, where aT is the electronic contribution and bT^3 is the phononic contribution, in a low-temperature regime (above the magnetic transition temperature).

It has been found that lattice thermal conductivity is negligible in comparison with electronic thermal conductivity at low temperatures. These finding not only deepens our understanding of Weyl semimetals but may also hold great promise for future applications in condensed matter physics.

4.2 Authors statement and publication 2

Name and surname: Pardeep Kumar
MagToP (ON6.6, Weyl group)
Institute of Physics, Polish academy of sciences,
Aleja Lotnikow 32/46, Warsaw, 02-668, Poland

STATEMENT

I declare that I am a co-author of the publication:

P.K. Tanwar, M.Ahmad, M.S. Alam, X.Yao, F.Tafti, and M. Matusiak, Gravitational anomaly in the ferrimagnetic topological Weyl semimetal NdAlSi. Phys. Rev. B 106, 108, L161106 (2023).

I contributed to the following:

- Prepared the thermal transport setup under the mentorship of Dr. hab. Marcin Matusiak
- Conducted experimental measurements, including electrical and thermal conductivity measurements, at temperatures as low as helium temperature and magnetic fields up to 14.5 T
- Developed Python software for analyzing the results obtained from electrical and thermal measurements
- Contributed in interpreting the experimental results
- Participate in conceptualizing the idea of gravitational anomaly
- Worked on writing the original manuscript and reviewed and edited it.
- Addressed the criticisms raised by the reviewers during the review process

Place: Warsaw

Date and Signature:

20/04/2024

Name and surname: Mujeeb Ahmad
MagToP (ON6.6, Weyl group)
Institute of Physics, Polish academy of sciences,
Aleja Lotnikow 32/46, Warsaw, 02-668, Poland

STATEMENT

I declare that I am a co-author of the publication:

P.K. Tanwar, M.Ahmad, M.S. Alam, X.Yao, F.Tafti, and M. Matusiak, Gravitational anomaly in the ferrimagnetic topological Weyl semimetal NdAlSi. Phys. Rev. B 106, *108*, L161106 (2023).

I contributed to the following: I performed electrical measurements with Mr. Pardeep Kumar Tanwar in this study and edited the manuscript.

Place: Warsaw

Date and Signature:

Mujeeb Ahmad
24/04/2024

Name and surname: Md Shahin Alam
MagToP (ON6.6, Weyl group)
Institute of Physics, Polish academy of sciences,
Aleja Lotnikow 32/46, Warsaw, 02-668, Poland

STATEMENT

I declare that I am a co-author of the publication:

P.K. Tanwar, M.Ahmad, M.S. Alam, X.Yao, F.Tafti, and M. Matusiak, Gravitational anomaly in the ferrimagnetic topological Weyl semimetal NdAlSi. Phys. Rev. B 106, *108,* L161106 (2023).

I contributed to the following:

- ✓ Discussion of the experimental results
- ✓ Writing section- Review & Editing

Place: Islampur, India

Date and Signature: 13/04/2024
Md. Shahin Alam.

Name and surname: Xiaohan Yao
Department of Physics, Boston College,
Chestnut Hill, Massachusetts 02467, USA

STATEMENT

I declare that I am a co-author of the publication:

P.K. Tanwar, M.Ahmad, M.S. Alam, X.Yao, F.Tafti, and M. Matusiak, Gravitational anomaly in the ferrimagnetic topological Weyl semimetal NdAlSi. Phys. Rev. B 106, *108*, L161106 (2023).

I contributed to the following:

- Synthesis of NdAlSi crystals
- Heat capacity measurements on NdAlSi and LaAlSi
- Review and editing of the manuscript

Place: Boston College

Date and Signature: 2/5/2024

Xiaohan Yao

Name and surname: Dr. Fazel Tafti
Department of Physics, Boston College,
Chestnut Hill, Massachusetts 02467, USA

STATEMENT

I declare that I am a co-author of the publication:

P.K. Tanwar, M.Ahmad, M.S. Alam, X.Yao, F.Tafti, and M. Matusiak, Gravitational anomaly in the ferrimagnetic topological Weyl semimetal NdAlSi. Phys. Rev. B 106, *108*, L161106 (2023).

I contributed to the following:

- Provided the crystals of NdAlSi
- Heat capacity measurements on NdAlSi and LaAlSi
- Review and editing of the manuscript

Place: Boston College

Date and Signature: 2/5/2024

Fazel

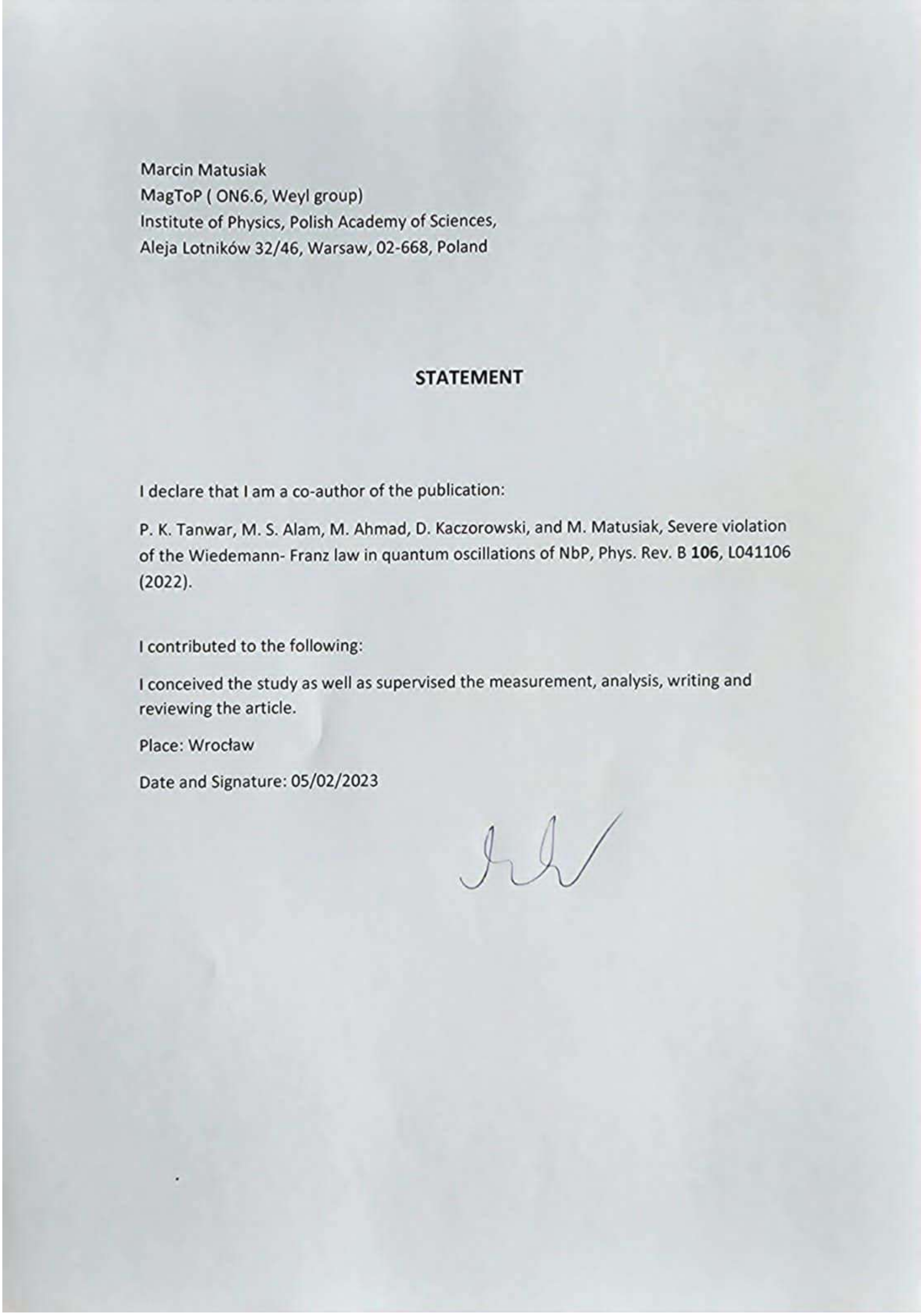

Marcin Matusiak
MagToP (ON6.6, Weyl group)
Institute of Physics, Polish Academy of Sciences,
Aleja Lotników 32/46, Warsaw, 02-668, Poland

STATEMENT

I declare that I am a co-author of the publication:

P. K. Tanwar, M. S. Alam, M. Ahmad, D. Kaczorowski, and M. Matusiak, Severe violation of the Wiedemann- Franz law in quantum oscillations of NbP, Phys. Rev. B **106**, L041106 (2022).

I contributed to the following:

I conceived the study as well as supervised the measurement, analysis, writing and reviewing the article.

Place: Wrocław

Date and Signature: 05/02/2023

Chapter 5

Summary

This Ph.D. project aimed at detecting topological excitations in Weyl semimetals. These materials are characterized by non-trivial electronic bands that linearly disperse and cross in energy-momentum space at points/nodes called Weyl points. These nodes come in pairs with opposite chirality defined by spin-momentum locking. Due to such spin-momentum locking, Weyl semimetals can potentially be employed in cutting-edge electronic devices for high-speed computing and developing advanced electronic components.

Weyl semimetals also host low-energy topological excitations in the vicinity of Weyl nodes, and some of these excitations are found to be charge-neutral. These charge-neutral excitations are impossible to study by electrical transport, but because they can transfer heat, measuring thermal properties can provide invaluable information about the system. The thermal phenomena also appear resistant to various detrimental effects, which may make the electrical transport results ambiguous. For instance, the current jetting does not affect the thermal conductivity as no direct external electrical current is applied. Thus, thermal transport can provide artifact-free information about quantum anomalies.

This thesis also involved the preparation of the experimental rig for heat transport measurements. The setup was designed to measure the thermal conductivity of bulk samples from room temperature down to liquid helium temperatures and in a magnetic field up to 14.5 T. Type-E thermocouples (constantan-chromel) was utilized and calibrated for temperatures from 3 to 300 K, and magnetic fields up to 14.5 T. To mitigate heat losses, we encapsulated the setup with a thermal shield to minimize radiation, covered it with a brass vacuum can to reduce diffusion, and used double-long phosphorous-bronze wire in coil form to minimize conduction losses.

In this thesis, the following questions about heat transport in Weyl semimetals are attempted to answer:

- Can topological excitations in Weyl semimetal carry heat but not charge?
  In Weyl semimetals with multiple pairs of Weyl points, an acoustic collective mode called chiral zero sound may emerge. This type of excitation is expected to carry heat but not an electrical charge. One anticipated experimental evidence of this excitation is huge quantum oscillations in magneto-thermal conductivity. Indeed, we observed this effect in NbP Weyl semimetal, which has multiple pairs of Weyl points. Chiral zero sound modes drastically violate the Wiedemann-Franz law.

- How does the magnetic field influence the properties of topological heat carriers?
  We have probed the gravitational anomaly, a thermal counterpart of the chiral anomaly in magnetic Weyl semimetal NdAlSi. In the chiral anomaly effect, an imbalance in the chemical potential between the nodes of opposite chirality arises due to the difference in the population number of Weyl fermions. However, gravitational anomaly stems from the thermal energy flow due to an imbalance of temperature between the nodes of opposite chirality, while the number of particular chirality Weyl fermions remains the same in respective nodes. The macroscopic manifestation of chiral anomaly is realized as increased electrical conductivity when a Weyl semimetal is subjected to parallel electrical and magnetic fields. In the case of gravitational anomaly, when the temperature gradient is applied instead of electrical current parallel to a magnetic field, thermal conductivity increases. Such behavior was observed in NdAlSi at low temperatures and in the high magnetic field.

- Is the Wiedemann-Franz law obeyed by Weyl fermions?
  The Wiedemann-Franz (WF) law is derived from the principles of classical physics and the Drude model of electron motion in metals. It holds well for many conductive materials, particularly metals, but may not apply to all materials under extreme conditions or in certain contexts, such as strongly correlated electron sys-

tems. However, Weyl fermions carry an anomalous heat current in the presence of a magnetic field and lead to an increase in thermal conductivity, which is proportional to the increase in electrical conductivity. In conclusion: yes, Weyl fermions obey the WF law in NdAlSi.

In conclusion, we have studied the topological Weyl semimetals through transport measurement and detected the two topological excitations: 1) chiral zero sound in NbP and 2) gravitational anomaly in NdAlSi. The discovery and examination of these findings have enriched the topological field by shedding light on new potential topological excitations. This thesis presents a manifestation of quantum field theory phenomena in solid-state systems.

Bibliography

[1] Claudia Felser and Johannes Gooth. “Topology and chirality”. In: *CHIRAL MATTER: Proceedings of the Nobel Symposium 167* (2023), pp. 115–141.

[2] Ming-Che Chang and Qian Niu. “Berry phase, hyperorbits, and the Hofstadter spectrum: Semiclassical dynamics in magnetic Bloch bands”. In: *Physical Review B* 53.11 (1996), p. 7010.

[3] Robert Karplus and JM Luttinger. “Hall effect in ferromagnetics”. In: *Physical Review* 95.5 (1954), p. 1154.

[4] T Jungwirth, Qian Niu, and AH MacDonald. “Anomalous Hall effect in ferromagnetic semiconductors”. In: *Physical review letters* 88.20 (2002), p. 207208.

[5] Kostya S Novoselov et al. “Unconventional quantum Hall effect and Berrys phase of 2π in bilayer graphene”. In: *Nature physics* 2.3 (2006), pp. 177–180.

[6] Di Xiao, Wang Yao, and Qian Niu. “Valley-contrasting physics in graphene: magnetic moment and topological transport”. In: *Physical review letters* 99.23 (2007), p. 236809.

[7] Binghai Yan and Claudia Felser. “Topological materials: Weyl semimetals”. In: *Annual Review of Condensed Matter Physics* 8 (2017), pp. 337–354.

[8] Michael Victor Berry. “Quantal phase factors accompanying adiabatic changes”. In: *Proceedings of the Royal Society of London. A. Mathematical and Physical Sciences* 392.1802 (1984), pp. 45–57.

[9] MV Berry. “Aspects of degeneracy”. In: *Chaotic Behavior in Quantum Systems: Theory and Applications*. Springer, 1985, pp. 123–140.

[10] Kai-Yu Yang, Yuan-Ming Lu, and Ying Ran. “Quantum Hall effects in a Weyl semimetal: Possible application in pyrochlore iridates”. In: *Physical Review B* 84.7 (2011), p. 075129.

[11] Andrew C Potter, Itamar Kimchi, and Ashvin Vishwanath. “Quantum oscillations from surface Fermi arcs in Weyl and Dirac semimetals”. In: *Nature communications* 5.1 (2014), p. 5161.

[12] Stephen L Adler. “Axial-vector vertex in spinor electrodynamics”. In: *Physical Review* 177.5 (1969), p. 2426.

[13] John Stewart Bell and Roman W Jackiw. “A PCAC puzzle”. In: *Nuovo cimento* 60.CERN-TH-920 (1969), pp. 47–61.

[14] Holger Bech Nielsen and Masao Ninomiya. “The Adler-Bell-Jackiw anomaly and Weyl fermions in a crystal”. In: *Physics Letters B* 130.6 (1983), pp. 389–396.

[15] Ari M Turner, Ashvin Vishwanath, and Chapter Outline Head. “Beyond band insulators: topology of semimetals and interacting phases”. In: *Topological Insulators* 6 (2013), p. 293.

[16] Pavan Hosur and Xiaoliang Qi. “Recent developments in transport phenomena in Weyl semimetals”. In: *Comptes Rendus Physique* 14.9-10 (2013), pp. 857–870.

[17] Niels BM Schröter et al. “Observation and control of maximal Chern numbers in a chiral topological semimetal”. In: *Science* 369.6500 (2020), pp. 179–183.

[18] K v Klitzing, Gerhard Dorda, and Michael Pepper. “New method for high-accuracy determination of the fine-structure constant based on quantized Hall resistance”. In: *Physical review letters* 45.6 (1980), p. 494.

[19] Klaus Von Klitzing. “Developments in the quantum Hall effect”. In: *Philosophical Transactions of the Royal Society A: Mathematical, Physical and Engineering Sciences* 363.1834 (2005), pp. 2203–2219.

[20] Daniel C Tsui, Horst L Stormer, and Arthur C Gossard. “Two-dimensional magnetotransport in the extreme quantum limit”. In: *Physical Review Letters* 48.22 (1982), p. 1559.

[21] Xiao-Gang Wen. “Topological orders and edge excitations in fractional quantum Hall states”. In: *Advances in Physics* 44.5 (1995), pp. 405–473.

[22] M Zahid Hasan and Charles L Kane. “Colloquium: topological insulators”. In: *Reviews of modern physics* 82.4 (2010), p. 3045.

[23] CH Li et al. “Electrical detection of charge-current-induced spin polarization due to spin-momentum locking in Bi2Se3”. In: *Nature nanotechnology* 9.3 (2014), pp. 218–224.

[24] Gordon W Semenoff. “Condensed-matter simulation of a three-dimensional anomaly”. In: *Physical Review Letters* 53.26 (1984), p. 2449.

[25] Kostya S Novoselov et al. “Two-dimensional gas of massless Dirac fermions in graphene”. In: *nature* 438.7065 (2005), pp. 197–200.

[26] AA Burkov, MD Hook, and Leon Balents. “Topological nodal semimetals”. In: *Physical Review B* 84.23 (2011), p. 235126.

[27] Chen Fang et al. “Topological nodal line semimetals”. In: *Chinese Physics B* 25.11 (2016), p. 117106.

[28] Xiangang Wan et al. “Topological semimetal and Fermi-arc surface states in the electronic structure of pyrochlore iridates”. In: *Physical Review B* 83.20 (2011), p. 205101.

[29] Ling Lu et al. “Experimental observation of Weyl points”. In: *Science* 349.6248 (2015), pp. 622–624.

[30] Hermann Weyl et al. “Electron and gravitation”. In: *z. Phys* 56 (1929), pp. 330–352.

[31] Takaaki Kajita. “Nobel Lecture: Discovery of atmospheric neutrino oscillations”. In: *Reviews of Modern Physics* 88.3 (2016), p. 030501.

[32] Arthur B McDonald. “Nobel lecture: the Sudbury Neutrino Observatory: observation of flavor change for solar neutrinos”. In: *Reviews of Modern Physics* 88.3 (2016), p. 030502.

[33] Zhong Fang et al. “The anomalous Hall effect and magnetic monopoles in momentum space”. In: *Science* 302.5642 (2003), pp. 92–95.

[34] Grigory E Volovik. *The universe in a helium droplet*. Vol. 117. OUP Oxford, 2003.

[35] Xiangang Wan et al. “Topological semimetal and Fermi-arc surface states in the electronic structure of pyrochlore iridates”. In: *Physical Review B* 83.20 (2011), p. 205101.

[36] NP Armitage, EJ Mele, and Ashvin Vishwanath. “Weyl and Dirac semimetals in three-dimensional solids”. In: *Reviews of Modern Physics* 90.1 (2018), p. 015001.

[37] Holger Bech Nielsen and Masao Ninomiya. “Absence of neutrinos on a lattice:(I). Proof by homotopy theory”. In: *Nuclear Physics B* 185.1 (1981), pp. 20–40.

[38] Leon Balents. “Weyl electrons kiss”. In: *Physics* 4 (2011), p. 36.

[39] FDM Haldane. “Attachment of surface" fermi arcs" to the bulk fermi surface:" fermi-level plumbing" in topological metals”. In: *arXiv preprint arXiv:1401.0529* (2014).

[40] Edward Witten. “Three lectures on topological phases of matter”. In: *La Rivista del Nuovo Cimento* 39 (2016), pp. 313–370.

[41] Varghese Mathai and Guo Chuan Thiang. “Global topology of Weyl semimetals and Fermi arcs”. In: *Journal of Physics A: Mathematical and Theoretical* 50.11 (2017), 11LT01.

[42] Su-Yang Xu et al. “Discovery of a Weyl fermion semimetal and topological Fermi arcs”. In: *Science* 349.6248 (2015), pp. 613–617.

[43] Hemian Yi et al. “Evidence of topological surface state in three-dimensional Dirac semimetal Cd3As2”. In: *Scientific Reports* 4.1 (2014), p. 6106.

[44] Philip JW Moll et al. “Transport evidence for Fermi-arc-mediated chirality transfer in the Dirac semimetal Cd3As2”. In: *Nature* 535.7611 (2016), pp. 266–270.

[45] Alexey A Soluyanov et al. “Type-ii weyl semimetals”. In: *Nature* 527.7579 (2015), pp. 495–498.

[46] Kentaro Ueda et al. “Magnetic-field induced multiple topological phases in pyrochlore iridates with Mott criticality”. In: *Nature communications* 8.1 (2017), p. 15515.

[47] Max Hirschberger et al. “The chiral anomaly and thermopower of Weyl fermions in the half-Heusler GdPtBi”. In: *Nature materials* 15.11 (2016), pp. 1161–1165.

[48] Cong Li et al. “Emergence of Weyl fermions by ferrimagnetism in a noncentrosymmetric magnetic Weyl semimetal”. In: *Nature Communications* 14.1 (2023), p. 7185.

[49] Peigang Li et al. “Giant room temperature anomalous Hall effect and tunable topology in a ferromagnetic topological semimetal Co2MnAl”. In: *Nature communications* 11.1 (2020), p. 3476.

[50] Kaustuv Manna et al. “From colossal to zero: controlling the anomalous Hall effect in magnetic Heusler compounds via Berry curvature design”. In: *Physical Review X* 8.4 (2018), p. 041045.

[51] Jonathan Noky et al. “Giant anomalous Hall and Nernst effect in magnetic cubic Heusler compounds”. In: *npj Computational Materials* 6.1 (2020), p. 77.

[52] Jürgen Kübler and Claudia Felser. “Non-collinear antiferromagnets and the anomalous Hall effect”. In: *Europhysics Letters* 108.6 (2014), p. 67001.

[53] Fangdong Tang et al. “Three-dimensional quantum Hall effect and metal–insulator transition in ZrTe5”. In: *Nature* 569.7757 (2019), pp. 537–541.

[54] Jin-Feng Wang et al. “Quantum oscillations in the magnetic Weyl semimetal NdAlSi arising from strong Weyl fermion–4 f electron exchange interaction”. In: *Physical Review B* 108.2 (2023), p. 024423.

[55] Gaoshang Gong et al. “Large topological Hall effect near room temperature in non-collinear ferromagnet La Mn 2 Ge 2 single crystal”. In: *Physical Review Materials* 5.3 (2021), p. 034405.

[56] Xiaohan Yao et al. “Large topological hall effect and spiral magnetic order in the Weyl Semimetal SmAlSi”. In: *Physical Review X* 13.1 (2023), p. 011035.

[57] Jonathan Gaudet et al. “Weyl-mediated helical magnetism in NdAlSi”. In: *Nature materials* 20.12 (2021), pp. 1650–1656.

[58] Andreas Kreyssig et al. “Magnetic order in GdBiPt studied by x-ray resonant magnetic scattering”. In: *Physical Review B* 84.22 (2011), p. 220408.

[59] RA Müller et al. “Magnetic structure of GdBiPt: A candidate antiferromagnetic topological insulator”. In: *Physical Review B* 90.4 (2014), p. 041109.

[60] Fei-Ye Li et al. “Weyl magnons in breathing pyrochlore antiferromagnets”. In: *Nature communications* 7.1 (2016), p. 12691.

[61] Tao Qin, Jianhui Zhou, and Junren Shi. “Berry curvature and the phonon Hall effect”. In: *Physical Review B* 86.10 (2012), p. 104305.

[62] MS Dresselhaus. “Transport Properties of Solids”. In: *Lecture Notes. In:-Solid State Physics-Part 1.)()* (2001).

[63] Neil W Ashcroft and N David Mermin. *Solid state physics*. Cengage Learning, 2022.

[64] Charles Kittel and Ching-yao Fong. *Quantum theory of solids*. Vol. 5. Wiley New York, 1963.

[65] Mazhar N Ali et al. “Large, non-saturating magnetoresistance in WTe2”. In: *Nature* 514.7521 (2014), pp. 205–208.

[66] Wei Zhang et al. “Topological aspect and quantum magnetoresistance of β- Ag 2 Te”. In: *Physical review letters* 106.15 (2011), p. 156808.

[67] R Xu et al. “Large magnetoresistance in non-magnetic silver chalcogenides”. In: *Nature* 390.6655 (1997), pp. 57–60.

[68] Tian Liang et al. “Ultrahigh mobility and giant magnetoresistance in the Dirac semimetal Cd 3 As 2”. In: *Nature materials* 14.3 (2015), pp. 280–284.

[69] A Narayanan et al. “Linear magnetoresistance caused by mobility fluctuations in n-doped Cd 3 As 2”. In: *Physical Review Letters* 114.11 (2015), p. 117201.

[70] Chandra Shekhar et al. “Extremely large magnetoresistance and ultrahigh mobility in the topological Weyl semimetal candidate NbP”. In: *Nature Physics* 11.8 (2015), pp. 645–649.

[71] AA Abrikosov. “Quantum magnetoresistance”. In: *Physical Review B* 58.5 (1998), p. 2788.

[72] David Shoenberg. *Magnetic oscillations in metals*. Cambridge University Press, 2009.

[73] Lawrence S Lerner. “Shubnikov-de Haas effect in bismuth”. In: *Physical Review* 127.5 (1962), p. 1480.

[74] JW McClure. “Diamagnetism of graphite”. In: *Physical Review* 104.3 (1956), p. 666.

[75] Tsuneya Ando. “Physics of graphene: zero-mode anomalies and roles of symmetry”. In: *Progress of Theoretical Physics Supplement* 176 (2008), pp. 203–226.

[76] Jin Hu et al. “Transport of topological semimetals”. In: *Annual Review of Materials Research* 49 (2019), pp. 207–252.

[77] Maxim N Chernodub et al. “Thermal transport, geometry, and anomalies”. In: *Physics Reports* 977 (2022), pp. 1–58.

[78] Qiang Li and Dmitri E Kharzeev. “Chiral magnetic effect in condensed matter systems”. In: *Nuclear Physics A* 956 (2016), pp. 107–111.

[79] Anton Yu Alekseev, Vadim V Cheianov, and Jürg Fröhlich. “Universality of transport properties in equilibrium, the goldstone theorem, and chiral anomaly”. In: *Physical review letters* 81.16 (1998), p. 3503.

[80] DT Son and BZ Spivak. “Chiral anomaly and classical negative magnetoresistance of Weyl metals”. In: *Physical Review B* 88.10 (2013), p. 104412.

[81] Cheng-Long Zhang et al. “Signatures of the Adler–Bell–Jackiw chiral anomaly in a Weyl fermion semimetal”. In: *Nature communications* 7.1 (2016), pp. 1–9.

[82] AA Burkov. “Chiral anomaly and transport in Weyl metals”. In: *Journal of Physics: Condensed Matter* 27.11 (2015), p. 113201.

[83] Dam Thanh Son and Naoki Yamamoto. “Berry curvature, triangle anomalies, and the chiral magnetic effect in Fermi liquids”. In: *Physical review letters* 109.18 (2012), p. 181602.

[84] Joon Sang Kang et al. “Large and Optimized Thermal Chiral Anomaly in Weyl Semimetal Bi-Sb”. In: *Physical Review Applied* 20.3 (2023), p. 034014.

[85] Alfred Brian Pippard. *Magnetoresistance in metals*. Vol. 2. Cambridge university press, 1989.

[86] Frank Arnold et al. “Negative magnetoresistance without well-defined chirality in the Weyl semimetal TaP”. In: *Nature communications* 7.1 (2016), p. 11615.

[87] RD Dos Reis et al. “On the search for the chiral anomaly in Weyl semimetals: the negative longitudinal magnetoresistance”. In: *New Journal of Physics* 18.8 (2016), p. 085006.

[88] Johannes Gooth et al. “Experimental signatures of the mixed axial–gravitational anomaly in the Weyl semimetal NbP”. In: *Nature* 547.7663 (2017), pp. 324–327.

[89] Jean Baptiste Joseph Baron Fourier et al. *The analytical theory of heat*. Courier Corporation, 2003.

[90] Ludwig Boltzmann. “Further studies on the heat balance among gas molecules”. In: *Kinetic Theory II* (1970), pp. 115–225.

[91] Charles Kittel. *Introduction to solid state physics*. John Wiley & sons, inc, 2005.

[92] Ch Kittel. “Interaction of spin waves and ultrasonic waves in ferromagnetic crystals”. In: *Physical Review* 110.4 (1958), p. 836.

[93] Alexandre Jaoui et al. “Departure from the Wiedemann–Franz law in WP2 driven by mismatch in T-square resistivity prefactors”. In: *npj Quantum Materials* 3.1 (2018), p. 64.

[94] JM Ziman. “Electrons and phonons (Clarendon Press, Oxford)”. In: (1960).

[95] James Bethin and Wendell S Williams. “Ambipolar Diffusion Contribution to High-Temperature Thermal Conductivity of Titanium Carbide”. In: *Journal of the American Ceramic Society* 60.9-10 (1977), pp. 424–427.

[96] J Heremans et al. “Electrical and thermal transport properties of arsenic”. In: *Journal of Physics C: Solid State Physics* 10.22 (1977), p. 4511.

[97] Alexandre Jaoui, Benot Fauqué, and Kamran Behnia. “Thermal resistivity and hydrodynamics of the degenerate electron fluid in antimony”. In: *Nature Communications* 12.1 (2021), p. 195.

[98] Jesse Crossno et al. “Observation of the Dirac fluid and the breakdown of the Wiedemann-Franz law in graphene”. In: *Science* 351.6277 (2016), pp. 1058–1061.

[99] PG Klemens. “Thermal conductivity and lattice vibrational modes”. In: *Solid state physics*. Vol. 7. Elsevier, 1958, pp. 1–98.

[100] H Beck, PF Meier, and A Thellung. “Phonon hydrodynamics in solids”. In: *physica status solidi (a)* 24.1 (1974), pp. 11–63.

[101] Yo Machida et al. “Phonon hydrodynamics in bulk insulators and semi-metals”. In: *arXiv preprint arXiv:2402.14870* (2024).

[102] C Strohm, GLJA Rikken, and P Wyder. “Phenomenological evidence for the phonon Hall effect”. In: *Physical review letters* 95.15 (2005), p. 155901.

[103] Xiaokang Li et al. “Phonon thermal Hall effect in strontium titanate”. In: *Physical review letters* 124.10 (2020), p. 105901.

[104] Hyungyu Jin et al. “Phonon-induced diamagnetic force and its effect on the lattice thermal conductivity”. In: *Nature materials* 14.6 (2015), pp. 601–606.

[105] XF Sun et al. “Large magnetothermal effect and spin-phonon coupling in a parent insulating cuprate Pr 1.3 La 0.7 CuO 4”. In: *Physical Review B* 72.10 (2005), p. 104501.

[106] Pardeep Kumar Tanwar et al. “Gravitational anomaly in the ferrimagnetic topological Weyl semimetal NdAlSi”. In: *Physical Review B* 108.16 (2023), p. L161106.

[107] Clemens Schindler et al. “Anisotropic electrical and thermal magnetotransport in the magnetic semimetal GdPtBi”. In: *Physical Review B* 101.12 (2020), p. 125119.

[108] Dung D Vu et al. “Magnon gap mediated lattice thermal conductivity in MnBi 2 Te 4”. In: *Physical Review B* 108.14 (2023), p. 144402.

[109] Koen Vandaele et al. “Thermal spin transport and energy conversion”. In: *Materials Today Physics* 1 (2017), pp. 39–49.

[110] AI Akhiezer and LA Shishkin. “ON THE-THEORY OF THE THERMAL CONDUCTIVITY AND ABSORPTION OF SOUND IN FERROMAGNETIC DIELECTRICS”. In: *SOVIET PHYSICS JETP* 34.7 (1958).

[111] D Douthett and SA Friedberg. “Effects of a magnetic field on heat conduction in some ferrimagnetic crystals”. In: *Physical Review* 121.6 (1961), p. 1662.

[112] Stephen R Boona and Joseph P Heremans. “Magnon thermal mean free path in yttrium iron garnet”. In: *Physical Review B* 90.6 (2014), p. 064421.

[113] Hisanao Sato. “On the thermal conductivity of ferromagnetics”. In: *Progress of Theoretical Physics* 13.1 (1955), pp. 119–120.

[114] DJ Sanders and D Walton. “Effect of magnon-phonon thermal relaxation on heat transport by magnons”. In: *Physical Review B* 15.3 (1977), p. 1489.

[115] RL Douglass. “Heat transport by spin waves in yttrium iron garnet”. In: *Physical Review* 129.3 (1963), p. 1132.

[116] D Walton, JE Rives, and Q Khalid. “Thermal transport by coupled magnons and phonons in yttrium iron garnet at low temperatures”. In: *Physical Review B* 8.3 (1973), p. 1210.

[117] Takashi Kikkawa et al. “Magnon polarons in the spin Seebeck effect”. In: *Physical review letters* 117.20 (2016), p. 207203.

[118] Charles Kittel and Ching-yao Fong. *Quantum theory of solids*. Wiley, 1987.

[119] Junsen Xiang et al. “Giant magnetic quantum oscillations in the thermal conductivity of TaAs: indications of chiral zero sound”. In: *Physical Review X* 9.3 (2019), p. 031036.

[120] Zhida Song and Xi Dai. “Hear the sound of Weyl fermions”. In: *Physical Review X* 9.2 (2019), p. 021053.

[121] Pardeep Kumar Tanwar et al. “Severe violation of the Wiedemann-Franz law in quantum oscillations of NbP”. In: *Physical Review B* 106.4 (2022), p. L041106.

[122] Reinhold A Bertlmann. *Anomalies in quantum field theory*. Vol. 91. Oxford university press, 2000.

[123] Tohru Eguchi and Peter GO Freund. “Quantum gravity and world topology”. In: *Physical Review Letters* 37.19 (1976), p. 1251.

[124] Karl Landsteiner, Eugenio Megias, and Francisco Pena-Benitez. “Gravitational anomaly and transport phenomena”. In: *Physical review letters* 107.2 (2011), p. 021601.

[125] Gordon Baym and Christopher Pethick. “Landau Fermi-liquid theory: concepts and applications”. In: (2008).

[126] Lev Davidovich Landau. “The theory of a Fermi liquid”. In: *Sov. Phys. JETP* 3.6 (1957), p. 920.

[127] WR Abel, AC Anderson, and JC Wheatley. “Propagation of zero sound in liquid He 3 at low temperatures”. In: *Physical Review Letters* 17.2 (1966), p. 74.

[128] A.Alekseevich Abrikosov, Lev Petrovich Gorkov, and Igor Ekhielevich Dzyaloshinski. *Methods of quantum field theory in statistical physics*. Dover Publications, New York, 1975.

[129] Evgenii Mikhailovich Lifshitz and Lev Petrovich Pitaevskii. “Statistical physics: theory of the condensed state”. In: *Chap. 3*. Westview Press, Boulder, Colorado1994), 1994, pp. 143–201.

[130] S-K Yip and Tin-Lun Ho. “Zero sound modes of dilute Fermi gases with arbitrary spin”. In: *Physical Review A* 59.6 (1999), p. 4653.

[131] JM Luttinger. “Theory of thermal transport coefficients”. In: *Physical Review* 135.6A (1964), A1505.

[132] Dung Vu et al. “Thermal chiral anomaly in the magnetic-field-induced ideal Weyl phase of Bi1- x Sb x”. In: *Nature materials* 20.11 (2021), pp. 1525–1531.

[133] Dmitri E Kharzeev et al. *Strongly interacting matter in magnetic fields: a guide to this volume*. Springer, 2013.

[134] Roberto Fornari. *Single crystals of electronic materials: growth and properties*. Woodhead Publishing, 2018.

[135] PS Dutta. “Bulk growth of crystals of III–V compound semiconductors”. In: (2011).

[136] Geon-Tae Hwang et al. “A reconfigurable rectified flexible energy harvester via solid-state single crystal grown PMN–PZT”. In: *Advanced Energy Materials* 5.10 (2015), p. 1500051.

[137] Donald TJ Hurle. *Handbook of crystal growth*. Elsevier Science & Technology, 1993.

[138] Iva Milisavljevic and Yiquan Wu. “Current status of solid-state single crystal growth”. In: *BMC materials* 2 (2020), pp. 1–26.

[139] DM Duffy. “Grain boundaries in ionic crystals”. In: *Journal of Physics C: Solid State Physics* 19.23 (1986), p. 4393.

[140] William T Read and WJPR Shockley. “Dislocation models of crystal grain boundaries”. In: *Physical review* 78.3 (1950), p. 275.

[141] Govindhan Dhanaraj et al. *Springer handbook of crystal growth*. Vol. 2. Springer, 2010, Chapter 27.

[142] Heinz Pick. “Festkörperphysik”. In: *Naturwissenschaften* 41.15 (1954), pp. 346–354.

[143] S Mahajan. “Defects in semiconductors and their effects on devices”. In: *Acta materialia* 48.1 (2000), pp. 137–149.

[144] AE De Barr. “The applications of single crystals”. In: *Contemporary Physics* 2.6 (1961), pp. 409–422.

[145] B.M.R. Wanklyn. *Practical aspects of flux growth by spontaneous nucleation. In: Crystal Growth, Vol. 1, ed. by B.R. Pamplin*. Pergamon, Oxford, 1974, pp. 217 288.

[146] Zhen Wang et al. “Helicity-protected ultrahigh mobility Weyl fermions in NbP”. In: *Physical Review B* 93.12 (2016), p. 121112.

[147] Peter Rudolph. *Handbook of crystal growth: Bulk crystal growth*. Elsevier, 2014.

[148] Yaoshui Wang, P Bennema, and P Van Der Linden. “Double crucible method for the growth of large superconducting YBCO single crystals”. In: *Journal of crystal growth* 106.2-3 (1990), pp. 483–486.

[149] JP Remeika and W Morrison Jackson. “A method for growing barium titanate single crystals”. In: *Journal of the American Chemical Society* 76.3 (1954), pp. 940–941.

[150] ROBERT C LINARES. “Substitution of Aluminum and Gallium in Single-Crystal Yttrium Iron Garnets”. In: *Journal of the American Ceramic Society* 48.2 (1965), pp. 68–70.

[151] Bernard Dennis Cullity. *Elements of X-ray Diffraction*. Addison-Wesley Publishing, 1956.

[152] Bertram Eugene Warren. *X-ray Diffraction*. Courier Corporation, 1990.

[153] William Henry Bragg. “IX. Bakerian Lecture.X-rays and crystal structure”. In: *Philosophical Transactions of the Royal Society of London. Series A, Containing Papers of a Mathematical or Physical Character* 215.523-537 (1915), pp. 253–274.

[154] Larson AC Dreele RBV. *General structure analysis system (GSAS)*. Tech. rep. Los Alamos National Laboratory Report LAUR: 86-748, 2000.

[155] Brian H Toby and Robert B Von Dreele. “GSAS-II: the genesis of a modern open-source all purpose crystallography software package”. In: *Journal of Applied Crystallography* 46.2 (2013), pp. 544–549.

[156] IM Lifshitz and Am M Kosevich. “Theory of magnetic susceptibility in metals at low temperature”. In: *Zh. eksp. teor. Fiz* 29 (1955), pp. 730–742.

[157] LD Landau. “Diamagnetismus der metalle”. In: *Zeitschrift für Physik* 64 (1930), pp. 629–637.

Institute of Physics Polish Academy of Sciences (IFPAN)
Aleja Lotników 32/46, 02-668
Warsaw, Poland
`www.ifpan.edu.pl`

Dostępy do artykułów:

PHYSICAL REVIEW B **106**, L041106 (2022)

Severe violation of the Wiedemann-Franz law in quantum oscillations of NbP
Pardeep Kumar Tanwar , Md Shahin Alam, Mujeeb Ahmad, Dariusz Kaczorowski , and Marcin Matusiak

DOI: 10.1103/PhysRevB.106.L041106

PHYSICAL REVIEW B **108**, L161106 (2023)

Gravitational anomaly in the ferrimagnetic topological Weyl semimetal NdAlSi
Pardeep Kumar Tanwar , Mujeeb Ahmad, Md Shahin Alam , Xiaohan Yao, Fazel Tafti, and Marcin Matusiak

DOI: 10.1103/PhysRevB.108.L161106